Dependence of Retinal Pigment Epithelium Integrity on the NRF2–Heme Oxygenase-1 Axis

Yida Jiang,[1,2] Li-Juan Duan,[1] Jingbo Pi,[3] Yun-Zheng Le,[4] and Guo-Hua Fong[1,2]

[1]Center for Vascular Biology, University of Connecticut Health Center, Farmington, Connecticut, United States
[2]Department of Cell Biology, University of Connecticut Health Center, Farmington, Connecticut, United States
[3]School of Public Health, China Medical University, Shenyang, Liaoning, China
[4]Departments of Medicine, Cell Biology, and Ophthalmology and Harold Hamm Oklahoma Diabetes Center, University of Oklahoma Health Sciences Center, Oklahoma City, Oklahoma, United States

Purpose. Tight junctions (TJs) form the structural basis of retinal pigment epithelium (RPE) barrier functions. Although oxidative stress contributes to age-related macular degeneration, it is unclear how RPE TJ integrity is controlled by redox balance. In this study, we investigated the protective roles of nuclear factor erythroid 2–related factor 2 (NRF2), a transcription factor, and heme oxygenase-1 (HO1), a heme-degrading enzyme encoded by the NRF2 target gene *HMOX1*.

Methods. ARPE19 cell cultures and mice, including wild-type, $Nrf2^{-/-}$, and RPE-specific NRF2-deficient mice, were treated with chemicals that impose oxidative stress or impact heme metabolism. In addition, NRF2 and HO1 expression in ARPE19 cells was knocked down by siRNA. TJ integrity was examined by anti–zonula occludens-1 staining of cultured cells or flatmount RPE tissues from mice. RPE barrier functions were evaluated by transepithelium electrical resistance in ARPE19 cells and immunofluorescence staining for albumin or dextran in eye histological sections.

Results. TJ structures and RPE barrier functions were compromised due to oxidant exposure and NRF2 deficiency but were rescued by HO1 inducer. Furthermore, treatment with HO1 inhibitor or heme precursor is destructive to TJ structures and RPE barrier properties. Interestingly, both NRF2 and HO1 were upregulated under oxidative stress, probably as an adaptive response to mitigate oxidant-inflicted damages.

Conclusions. Our data indicate that the NRF2–HO1 axis protects TJ integrity and RPE barrier functions by driving heme degradation.

Keywords: oxidative stress, NRF2, heme oxygenase-1, retinal pigment epithelial cells, tight junctions, age-related macular degeneration

The retinal pigment epithelium (RPE) is a monolayer of cells located between the neuroretina and choroid vasculature,[1] and it serves as the outer blood–retinal barrier to control the exchange of nutrition and metabolic wastes between the two tissues. The RPE cells are polarized, with their basal side facing the choroid and numerous protrusions of the apical side pointing toward the adjacent photoreceptor cells. A thin layer of extracellular matrix, known as Bruch's membrane, separates the RPE from the choroid vasculature.[2,3]

The RPE barrier function is mostly supported by the tight junctions (TJs) between RPE cells. Structurally, TJs are formed through high-affinity interactions between the extracellular domains of occludins/claudins in neighboring cells and are stabilized by zona occludens, such as zona occludens-1 (ZO1), which link the intracellular domains of occludins/claudins to cytoskeletal fiber actin filaments.[4] Functionally, TJs prevent harmful molecules, pathogens, and cells (such as inflammatory leukocytes) in the choroid circulation from entering retinal tissues.[5–8]

Because the RPE barrier is impermeable to polar or charged molecules by diffusion, exchange between the choroid and retinal tissues depends on active transport,[9,10] which are highly energy-demanding processes. The main energy source for RPE cells is the β-oxidation of fatty acids, which are mostly derived from photoreceptor outer segments shed on a daily basis and endocytosed by RPE cells.[11–14] However, fatty acid oxidation produces large amounts of reactive oxygen species (ROS),[15–17] thus exposing RPE cells to the risk of oxidative stress.

Various conditions and events may tip the balance toward oxidative stress by promoting ROS production and/or suppressing antioxidant mechanisms. For example, elevated ROS production is associated with smoking,[18,19] exposure to blue light,[20] and consumption of oxidative diets.[21] Furthermore, the effectiveness of antioxidant mechanisms may decline with aging,[22] thus rendering RPE cells increasingly susceptible to oxidative stress. Consistent with this notion, NRF2 expression is reduced in older mice.[23] Increased oxidative stress and declining antioxidant functions are major

contributors to the deterioration of RPE barrier function and progression of age-related macular degeneration (AMD), or age-related retinal degeneration in mice due to the lack of the macular structure in these animals.[23–25]

To mitigate the destructive effects of ROS, healthy RPE cells, as well as other cell types, are equipped with antioxidant mechanisms, such as those mediated by nuclear factor erythroid factor 2–related factor 2 (NRF2).[25–30]

NRF2 is a transcription factor that activates the expression of many target genes by recognizing the antioxidant response elements in their regulatory sequences.[31] NRF2 target genes encode proteins that regulate several cellular processes, such as xenobiotic detoxification, redox balancing, heme metabolism, and NADPH production.[31] Despite these important functions, $Nrf2^{-/-}$ mice do not display overt developmental defects and are able to survive into old age.[32,33] However, $Nrf2^{-/-}$ mice have reduced tolerance to environmental stress.[34] In ocular tissues of $Nrf2^{-/-}$ mice, retinal degenerative phenotypes and cataracts develop at 12 and 21 months of age, respectively.[33,35] Specifically, 12-month-old $Nrf2^{-/-}$ mice exhibit subretinal deposition of lipid materials (lipofuscin), localized loss of RPE cells, and spontaneous choroidal neovascularization.[35] It remains unclear, however, how NRF2 deficiency initiates these events. In particular, it is unknown whether the structural integrity of RPE TJs is affected prior to the development of the more advanced phenotypes.

Among NRF2 downstream targets, of particular relevance to this study is the *Hmox1* gene, which encodes heme oxygenase-1 (HO1).[36–39] At the biochemical level, HO1 is an enzyme responsible for heme degradation, converting it into biliverdin, carbon monoxide, and iron (Fe^{++}).[40–42] Because heme promotes ROS production, whereas biliverdin and carbon monoxide are antioxidants, heme degradation by HO1 alleviates oxidative stress.[43–46] The role of HO1 in regulating TJ integrity of the RPE is unknown, although it was found to influence cell survival in ARPE19 cultures.[47–49] In mice, *Hmox1* knockout led to perinatal lethality in 80% of $Hmox1^{-/-}$ mice, with the remaining 20% suffering from very severe anemia due to low levels of serum iron.[50]

Although oxidative stress is known to cause RPE cell death,[48,51–57] its specific effects on TJs are not well characterized. In this study, we took a combination of in vitro and in vivo approaches to examine the effects of oxidative stress on the structural integrity and barrier functions of RPE TJs, and we investigated the roles of the NRF2–HO1 antioxidant pathway in this respect. Overall, our data indicate that oxidative stress had damaging effects on TJ integrity of the RPE, whereas the NRF2–HO1 axis was protective, in part via HO1-mediated heme degradation. According to a recent literature search, there are currently no published in vivo studies directly focused on the relationship between TJ integrity and redox regulation mechanisms. Therefore, studies described in this paper may represent the first in vivo analysis on this important subject.

METHODS

Chemical Treatment of ARPE19 Cells

ARPE19 cells were purchased from the American Type Culture Collection (CRL-2303; ATCC, Manassas, VA, USA) and were cultured in a 5% CO_2 incubator at 37°C. The culture medium was Gibco DMEM/F-12 medium (11330057; Thermo Fisher Scientific, Waltham, MA, USA) supplemented with 10% heat-inactivated fetal bovine serum (FBS) and Gibco Antibiotic-Antimycotic (100×) (15240096; Thermo Fisher Scientific). Approximately 4 hours before the addition of experimental chemicals, culture media were replaced with FBS-free DMEM/F-12. Chemical stocks were made in PBS, and final concentrations in the DMEM/F-12 media were as follows: sodium iodate ($NaIO_3$), 2 mM; cobalt protoporphyrin IX (CoPP), 5 µM; zinc protoporphyrin-9 (ZnPPIX), 5 µM; and hemin, 0.5 µM. The duration of chemical treatments was 16 hours, unless specified otherwise.

siRNA-Mediated Knockdown in ARPE19 Cells

Transfection of ARPE19 cells was carried out using Invitrogen Lipofectamine RNAiMAX (13778150; Thermo Fisher Scientific) according to manufacturer's instructions. *NRF2-* and *HMOX1* (HO1)-specific siRNA reagents were purchased as SMARTpools from Horizon Discovery (Cambridge, UK), and scrambled siRNA (negative control) was obtained from Thermo Fisher Scientific. Transfection was carried out when cultures were approximately 80% confluent. ARPE19 cells were harvested 48 hours after transfection for Western blotting or fixed 60 hours after transfection for immunofluorescence (IF) staining.

Immunofluorescence Staining of ARPE19 Cells

For IF staining, ARPE19 cells were cultured in 24-well plates to confluency, typically after being treated with chemicals or siRNA. ARPE19 cells were fixed in 4% paraformaldehyde (PFA). Fixed ARPE 19 cells were incubated at 4°C with primary antibodies (Supplementary Table S2) diluted in immunoblocking buffer (IBB), which consists of 1× PBS, 0.1% Triton X-100, and 1% BSA. After overnight incubation, cells were washed three times in PBS and incubated for 1 hour at room temperature with fluorophore-conjugated secondary antibodies (Supplementary Table S2) in IBB. Stained cells were washed with PBS three times and analyzed by fluorescence microscopy.

Transepithelial Electrical Resistance Assay

ARPE19 cells were cultured on Falcon Permeable Support for 24-well plates (353095; Corning, Inc., Corning, NY, USA), and monolayers were used for transepithelial electrical resistance (TEER) assay without fixation. These devices have transparent bottoms with 0.4-µm pores and are equivalent to Transwell inserts. Dulbecco's Modified Eagle's Medium (DMEM) was used as culture medium, supplemented with 10% heat-inactivated FBS and antibiotics. After confluency was reached, fresh monolayers were used for TEER assays without fixation. TEER measurements were performed using an Epithelial Volt/Ohm (TEER) Meter (World Precision Instruments, Sarasota, FL, USA) (see Fig. 3A). Where appropriate, ARPE19 cells were treated with ZnPPIX (5 µM), $NaIO_3$ (2 mM), CoPP (5 µM), and hemin (0.5 µM) before the TEER assays.

Mice

All animals were used according to protocols approved by the University of Connecticut Health Institutional Animal Care and Use Committee (IACUC) in compliance with Animal Welfare Assurance and in a manner that adhered to the ARVO Statement for the Use of Animals in Ophthalmic

and Vision Research. $Nrf2^{-/-}$ mice[32] were purchased from The Jackson Laboratories (017009; Bar Harbor, ME, USA), and maintained in C57BL/6 background. Floxed *Nrf2* (*Nrf2^{f/f}*) and P_{VMD2}-*rtTA::tetO*-P_{bCMV}-*cre* (*VMD2-cre*) mice were contributed by Jingbo Pi and Yun-Zheng Le,[58,59] respectively; *VMD2-cre* mice are also currently available at The Jackson Laboratories (032910). *Nrf2^{f/f}* mice were backcrossed to C57BL/6J-strain background for at least seven generations; *VMD2-cre* mice were originally generated in a FVB/N background but were backcrossed into C57BL/6J mice for four generations before being crossed with *Nrf2^{f/f}* mice.

Genotyping by PCR

Ear punch tissues were used for DNA extraction and genotype determination by PCR. Primers are listed in Supplementary Table S1. PCR reactions were carried out by standard protocols except that the annealing time was 3 minutes at each cycle.

Breeding for *Nrf2^{f/f}/VMD2-cre* Mice and Induction of VMD2-cre Expression

Nrf2^{f/f}/VMD2-cre × *Nrf2^{f/f}* breeding pairs were set up, and mothers were fed with doxycycline (Dox)-containing chow (0.675 g/kg of chow; Envigo, Indianapolis, IN, USA), starting the day a new litter was born and continuing for 3 weeks.

Determination of Deletion Efficiency by Quantitative RT-PCR

After doxycycline treatment, RPE cells were isolated from 3-week-old mice according to a published protocol[60] and were used for total RNA isolation. NRF2 mRNA levels were determined by quantitative RT-PCR using the NRF2-specific primers GTCATCAAAAAGCCCCATTCACA and GGGCGGC-GACTTTATTCTTACC, located in the floxed exon. The quantitative RT-PCR primers for β-actin were GGCTGTATTCCCC-CTCCATCG and CCAGTTGGTAACAATGCCATGT.

Administration of Experimental Compounds to Mice

All stock solutions were prepared in PBS. Dosages for intraperitoneal (IP) injection were 10 mg/kg for $NaIO_3$, 1 mg/kg for CoPP, and 1 mg/kg for hemin. Frequency and duration of injections are described where appropriate. For subretinal injection, one eye of each mouse was injected with a single dose of ZnPPIX or CoPP. In both cases, the concentration was 125 µM (dissolved in PBS), and the volume of injection was 1 µL. The contralateral eye was injected with 1 µL PBS.

Isolation of RPE–Choroid Tissues

Eyes were enucleated from euthanized mice and fixed in 100% methanol at room temperature for 1 hour. RPE–choroid tissues were physically separated from retina tissues, further fixed in 100% methanol for 1 hour, and then rinsed three times in PBS. RPE and choroid tissues remained attached to each other during and after isolation so the RPE sheet remained intact.

Wholemount Immunofluorescence Staining and Flatmount Imaging of RPE Tissues

Wholemount RPE tissues were incubated in IBB for 1 hour at room temperature. Blocked tissues were incubated at 4°C with primary antibodies diluted in IBB (Supplementary Table S2). After overnight incubation, tissues were washed three times in PBS and incubated for 1 hour at room temperature with fluorophore-conjugated secondary antibodies diluted in IBB (Supplementary Table S2). RPE tissues were then washed three times in PBS, flatmounted on precleaned glass slides (Fisherbrand ColorFrost; Thermo Fisher Scientific) and in VectaMount AQ (Vector Laboratories, Newark, CA, USA), and sealed under coverslips. Flatmounted tissues had the RPE side on top of the choroid and were analyzed by fluorescence microscopy.

RPE Permeability Analysis by Immunofluorescence Staining of Eye Frozen Sections

RPE permeability was evaluated by analyzing the cross-RPE diffusion of dextran (3 kD) injected into the systemic circulation. Briefly, biotin-labeled, lysine-conjugated dextran (1 mg/mL in PBS) was injected into the retro-orbital space (5 mg/kg). After 15 minutes, mice were euthanized by perfusion with ice-cold PBS and perfusion-fixed with 4% PFA. Eyes were enucleated, further fixed in 4% PFA at room temperature for 4 hours, and washed three times with PBS. Fixed eyeballs were equilibrated in 30% sucrose at 4°C overnight. Sucrose-equilibrated eyeballs were embedded in optimal cutting temperature (OCT) compound on dry ice, and 6-µm sections were cut at −20°C. Frozen sections were stained with Alexa Fluor 549 avidin (Supplementary Table S2).

RPE permeability was also analyzed by anti-mouse albumin IF staining of frozen eye sections prepared from perfusion-euthanized mice. For both Alexa Fluor 549 avidin and anti-albumin staining, sections were first blocked in IBB, but BSA was omitted for all steps of anti-albumin IF staining to minimize background signals. Incubation with Alexa Fluor 549 avidin and anti-albumin was carried out at 4°C overnight and, in the case of anti-albumin staining, secondary antibody incubation for 1 hour at room temperature. After the completion of antibody incubation, sections were washed three times with PBS, mounted in VectaMount AQ, and analyzed by fluorescence and brightfield microscopy.

Brightfield and Fluorescence Microscopy

Imaging of all tissue sections and RPE flatmounts was carried out using a Zeiss AxioCam MRm digital camera (Carl Zeiss Microscopy, Jena, Germany) attached to a Zeiss Axio Observer Z1. In each experiment, identical lighting and digital settings were set for control and experimental groups. At least three representative images were taken for each specimen.

Quantification of Fluorescence Pixel Values

Band intensities in Western blots and signals in IF-stained ARPE19 cells, RPE flatmounts, and retinal sections were quantified with the aid of ImageJ software (National Insti-

tutes of Health, Bethesda, MD, USA). ZO1 located at the intercellular junctions was quantified by a method described in Supplementary Figure S2. Briefly, intracellularly located ZO1$^+$ signals were erased, leaving behind only junctional ZO1$^+$ signals for ImageJ-assisted quantification. For quantification of IF-staining signals, the average pixel value of at least three representative areas of the same specimen was used as a single data point (n).

Western Blotting

Cultured ARPE19 cells or freshly isolated RPE–choroid tissues were lysed with radioimmunoprecipitation assay (RIPA) buffer (50-mM Tris hydrochloride [HCl], pH 8.0; 150-mM NaCl, 1% NP-40, 0.5% sodium deoxycholate, 0.1% SDS, 1-mM NaF, and 1-mM sodium orthovanadate) and boiled for 5 minutes in SDS gel loading buffer (250-mM Tris HCl, pH 6.8; 10% SDS; 30% [v/v] glycerol; 10-mM dithiothreitol [DTT]; and 0.05% [w/v] bromophenol blue). Proteins were separated in 10% SDS polyacrylamide gels and electrically transferred to polyvinylidene fluoride (PVDF) membrane (Immobilon-P PVDF Membrane, IPVH00010; MilliporeSigma, Burlington, MA, USA) in transfer buffer consisting of 25-mM Tris Cl, pH 8.0; 192-mM glycine; and 20% methanol. The PVDF membrane was blocked in blocking buffer containing 5% non-fat dry milk and then with primary antibody solution containing 5% BSA. After extensive washing with Tris-buffered saline with 0.1% Tween 20 (TBST), membranes were incubated with secondary antibody conjugated with horseradish peroxidase (Supplementary Table S2). Signals were detected using a digital

gel documentation system (Bio-Rad Laboratories, Hercules, CA, USA).

Statistical Analyses

For in vivo studies where both eyes were treated equally (such as in mice injected with CoPP intraperitoneally), the average value from both retinas in each mouse was used as a single datapoint. Where the contralateral eyes were differentially treated (such as subretinal injection of experimental compounds into one eye and vehicle into the other), data from each retina were used for statistical analysis. For cell culture–based studies, data from each individual cell culture were used as one datapoint. Quantifications were carried out with genotype or treatment masked to the investigator, except for TEER assays, where the data were automatically recorded by the instrument. Data were analyzed by two-tailed Student's t-tests or two-way ANOVA tests as indicated. Errors were calculated as standard error of the mean (SEM). $P < 0.05$ was considered statistically significant.

RESULTS

Injury of ARPE19 Cell TJs Due to Oxidant Exposure and NRF2 Knockdown

ARPE19 cells are spontaneously established human RPE cells.[61] When cultured to confluency, ARPE19 cells develop features reflective of TJs, such as localization of ZO1 at intercellular junctions.[61] To investigate whether TJ structures are sensitive to the damaging effects of NaIO$_3$-dependent
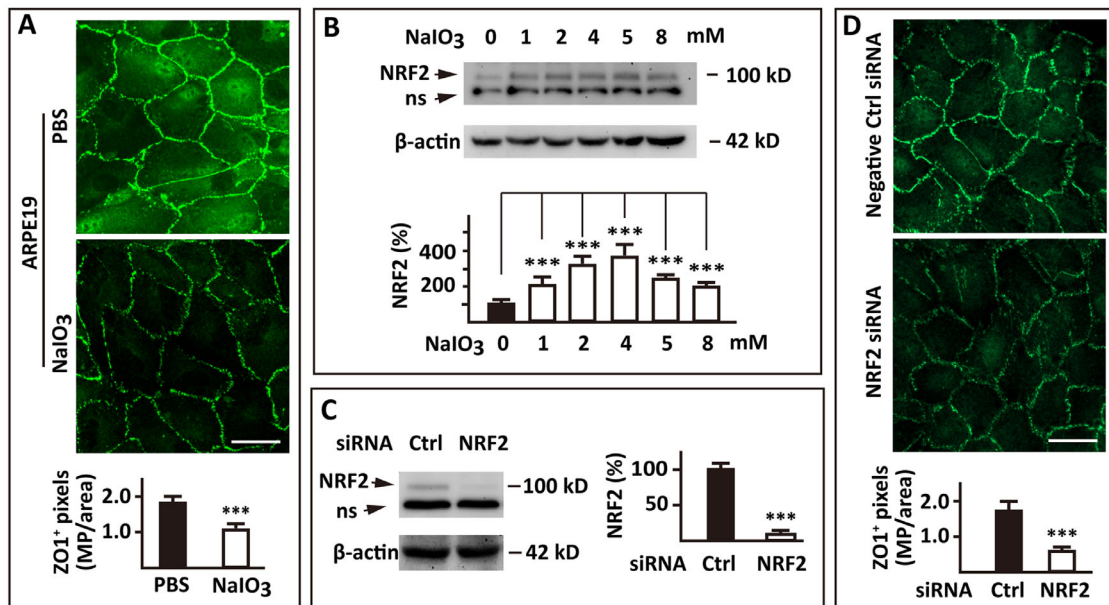

FIGURE 1. TJ damages in ARPE19 cells treated with NaIO$_3$ or *NRF2* siRNA. (**A**) Reduced ZO1 levels in NaIO$_3$-treated ARPE19 cells. Confluent ARPE19 cultures were treated with 2-mM NaIO$_3$ or vehicle (PBS). After 16 hours of treatment, anti-ZO1 IF staining was carried out, and fluorescence images were taken. MP/area, megapixels per 0.01 mm^2 culture area (applicable to all ARPE19 cell culture images in this manuscript); $n = 8$. (**B**) Elevated NRF2 protein levels in NaIO$_3$-treated ARPE19 cells. After 16 hours of treatment at the indicated concentrations, cells were lysed and analyzed by anti-NRF2 Western blotting. NRF2 (100-kD band) levels were all normalized to β-actin and are shown as percentage values relative to 0-mM control. ns, nonspecific band; $n = 3$. (**C**) Analysis of NRF2 protein levels in siRNA-transfected ARPE19 cells by Western blotting. NRF2 protein levels are shown as percentage values relative to scrambled siRNA-transfected cells; $n = 3$. (**D**) Reduced ZO1 levels in *NRF2* siRNA-transfected ARPE19 cell cultures. Negative control was scrambled siRNA. Anti-ZO1 IF staining was performed 2 days after transfection; $n = 6$. *Scale bars*: 30 µm (**A, B**). For statistical analyses, two-tailed Student's t-tests were applied. ***$P < 0.001$.
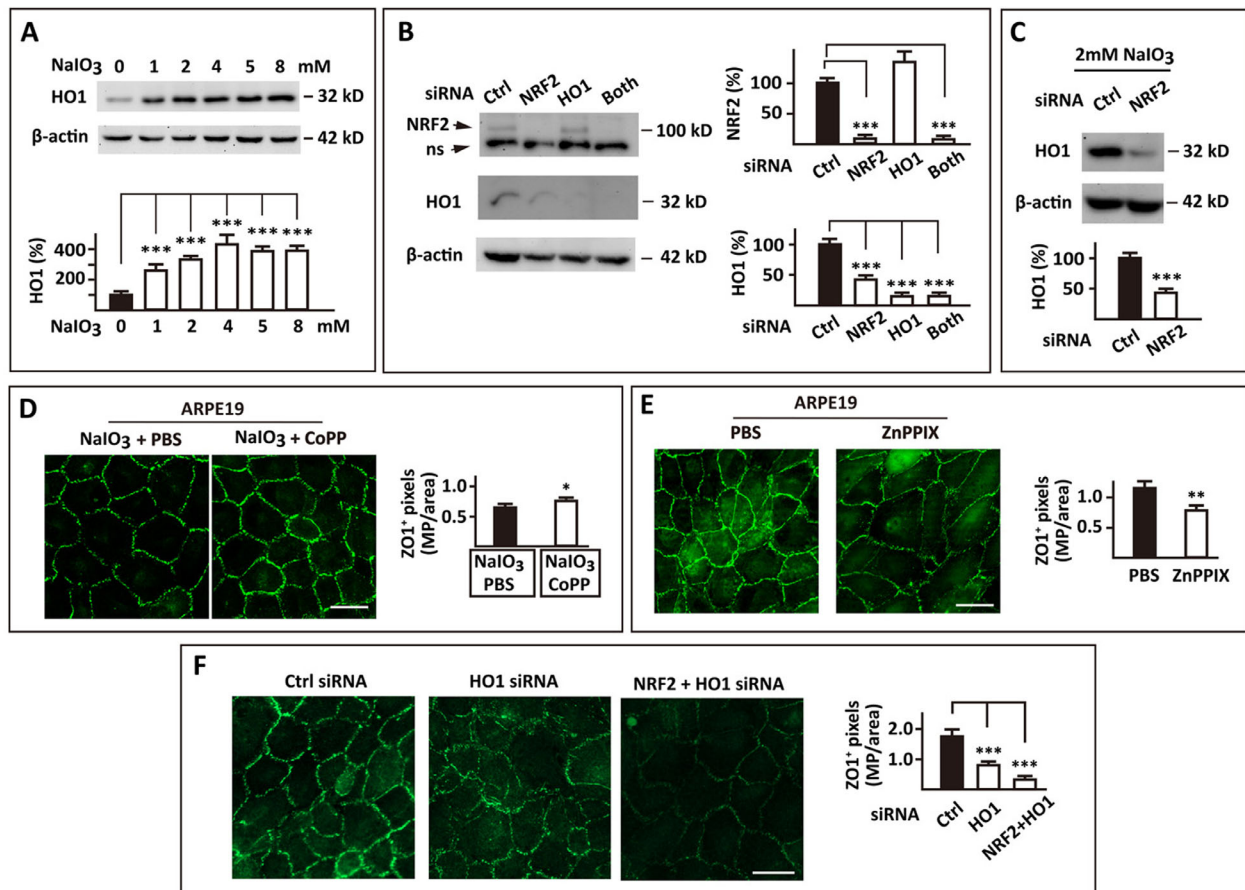
FIGURE 2. Role of HO1 in protecting ARPE19 cell TJ structures against oxidative stress. (**A**) Upregulation of HO1 expression by $NaIO_3$ treatment in ARPE19 cells. Anti-HO1 Western blotting was carried out after ARPE19 cells were treated for 16 hours with $NaIO_3$ (0–8 mM). HO1 band intensities were normalized against β-actin and are shown as percentage values relative to 0-mM control; $n = 3$. (**B**) Anti-HO1 Western blot of ARPE19 cells transfected with different siRNAs, including scrambled siRNA (Ctrl), *NRF2* siRNA, *HO1* siRNA, and a mixture of *NRF2* and *HO1* siRNA (Both). Cells were harvested for Western blotting 2 days after transfection. NRF2 and HO1 band intensities were normalized against β-actin and are shown as percentage values relative to scrambled siRNA-transfected controls; $n = 3$. (**C**) Anti-HO1 Western blot of ARPE19 cells transfected with NRF2 siRNA and treated with $NaIO_3$ for 16 hours; $n = 3$. (**D**) Protection of ARPE19 cell TJs by CoPP. ARPE19 cell cultures were treated for 16 hours with $NaIO_3$ + PBS or $NaIO_3$ + CoPP and were analyzed by anti-ZO1 IF staining; $n = 8$. (**E**) Disruption of ARPE19 cell TJ structures by the HO1 inhibitor ZnPPIX. ARPE19 cells were treated with ZnPPIX or PBS for 30 hours, fixed, and subject to anti-IF ZO1 staining; $n = 8$. (**F**) Requirement of HO1 for TJs in ARPE19 cell cultures. ARPE19 cells were transfected with different siRNAs as indicated above each image. Two days later, cells were analyzed by anti-ZO1 IF staining; $n = 8$. *Scale bars*: 30 µm. Data were analyzed using two-tailed Student's *t*-tests. *$P < 0.05$, **$P < 0.01$, ***$P < 0.001$.

oxidative stress, we started out by identifying a sublethal $NaIO_3$ concentration. We found that the vast majority of cells remained viable at 2 mM, with only rare exceptions (Supplementary Fig. S1). Therefore, oxidative stress in ARPE19 cultures was induced by supplementing the medium with 2-mM $NaIO_3$ for 16 hours, unless specified otherwise.

The integrity of TJ structures was assessed by anti-ZO1 IF staining. To specifically quantify junctional ZO1, intracellularly located ZO1^{+} signals were erased as explained in Supplementary Figure S2, leaving ZO1^{+} pixels at cell–cell junctions for quantification by ImageJ. As shown in Figure 1A, junctional ZO1^{+} pixels were significantly reduced in $NaIO_3$-treated cultures, suggesting that TJ structures were damaged under oxidative stress.

In addition to reduced levels of junctional ZO1, NRF2 protein levels were increased in ARPE19 cultures under oxidative stress (Fig. 1B). NRF2 upregulation peaked at 4 mM of $NaIO_3$, leveling off at higher concentrations, presumably because of decreased viability of ARPE19 cells at higher

$NaIO_3$ concentrations. To test if NRF2 was important to TJs, we carried out siRNA-mediated NRF2 knockdown. Transfection of ARPE19 cells with *NRF2*-specific siRNA reduced NRF2 protein levels to 7% of scrambled siRNA-transfected controls (Fig. 1C). In *NRF2* knockdown cells, junctional ZO1 levels were significantly reduced (Fig. 1D).

Role of HO1 in Protecting ARPE19 TJs Against Oxidative Stress

Under oxidative stress, HO1 protein levels were elevated in ARPE19 cells, plateauing at 4 mM of $NaIO_3$ (Fig. 2A). This phenomenon parallels NRF2 upregulation under similar conditions (Figs. 1B, 2A). Furthermore, *NRF2* knockdown in ARPE19 cells also led to downregulated HO1 expression, both under normal culture conditions and when exposed to $NaIO_3$ (Figs. 2B, 2C). These data are consistent with the *HMOX1* gene (which encodes HO1) being a downstream
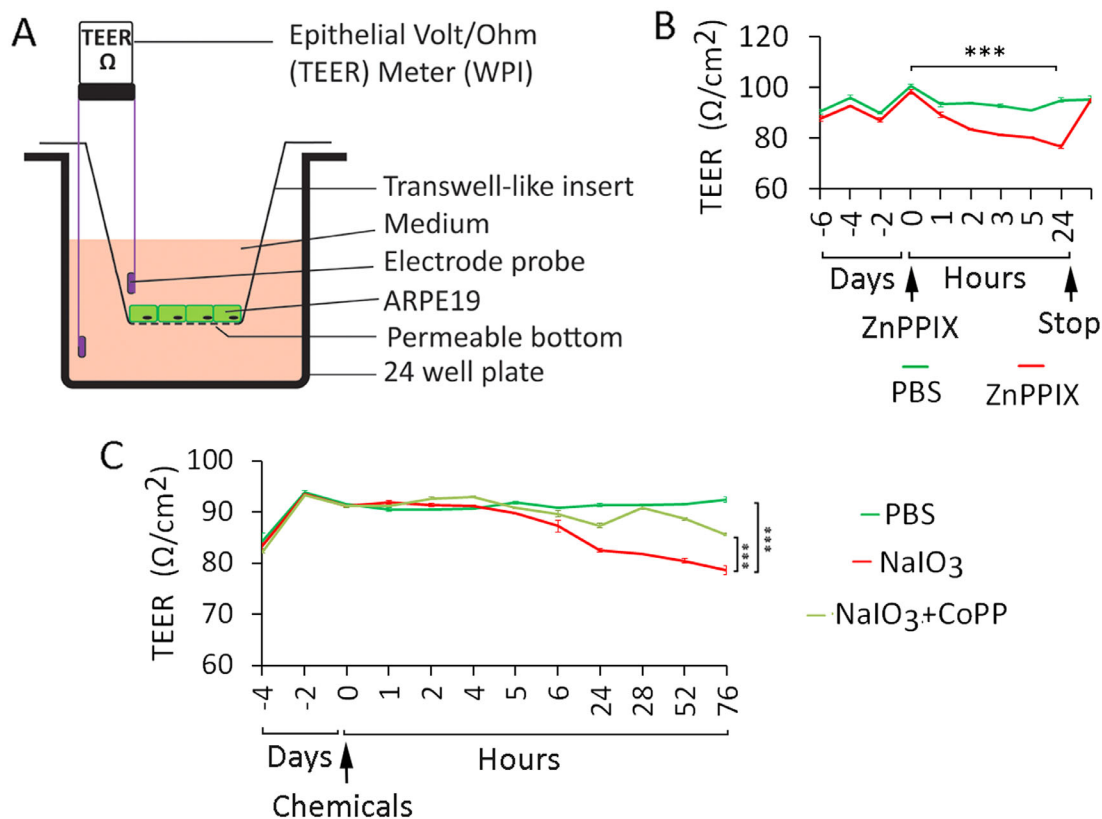
FIGURE 3. Role of HO1 in the maintenance of barrier functions of ARPE19 monolayer cultures. (**A**) Schematic description of the experimental set-up. ARPE19 cells were cultured in transparent, permeable, Transwell-like inserts set into 24-well plates (one well is shown). Cultures were allowed to reach confluency and develop barrier function before the addition of chemicals. (**B**) TEER measurements for ZnPPIX- or PBS-treated ARPE19 cell cultures, where -6, -4, and -2 days indicate the number of days before the addition of ZnPPIX. After ZnPPIX was added, TEER values were recorded at the indicated hours, with values at 0 hour being taken immediately before the addition of ZnPPIX. At 24 hours after the addition of ZnPPIX, treatment was stopped by replacing ZnPPIX-containing media with ZnPPIX-free media. (**C**) Rescue of barrier function by CoPP. Confluent ARPE19 cell cultures were treated for 76 hours with NaIO$_3$ (2 mM) or a combination of NaIO$_3$ (2 mM) and CoPP (5 μM), using PBS as vehicle. TEER values were measured before and after the addition of chemicals; $n = 3$. Data were analyzed by two-way ANOVA tests, comparing the curve in a chemically treated group to the vehicle group (**B**) or between the two curves indicated by a half bracket. ***$P < 0.001$.

target of NRF2[36,62,63] and indicate that HO1 expression in ARPE19 cells is dependent on NRF2, at least partially.

We speculated that HO1 might help mitigate, although not completely overcome, the TJ-damaging effects of oxidative stress. To test this possibility, we treated ARPE19 cells with CoPP, a well-characterized HO1 inducer,[64,65] and evaluated ZO1 levels by IF staining. Indeed, in NaIO$_3$-treated ARPE19 cell cultures, the inclusion of CoPP helped preserve ZO1 at intercellular junctions (Fig. 2D).

In a complementary experiment, we inhibited HO1 activity by treating ARPE19 cells with ZnPPIX, a previously validated competitive inhibitor of HO1.[66,67] In ZnPPIX-treated ARPE19 cells, ZO1 IF-staining intensity was significantly reduced at intercellular junctions (Fig. 2D). Overall, these data indicate that HO1 is important for TJ integrity.

To examine the role of HO1 more directly, ARPE19 cells were transfected with *HMOX1* (HO1)-specific siRNA, resulting in the reduction of HO1 protein levels to 14% of the values in scrambled siRNA-transfected cells (Fig. 2B). Similar to HO1 inhibitor treatment, HO1 knockdown also caused the breakdown of TJs (Fig. 2E), manifested as reduced ZO1$^+$ signals at the intercellular junctions. As expected, double knockdown of both NRF2 and HO1 damaged TJs even further (Fig. 2E).

Role of HO1 in ARPE19 Barrier Function

Because HO1 was found to be important for the structural integrity of TJs (Fig. 2E), we wondered if reduced HO1 activity would also functionally affect barrier properties. In confluent ARPE19 cell monolayers, the formation of TJs among neighboring cells contributes to barrier functions across the monolayer, which can be recorded as resistance to electrical currents in TEER assays, as depicted in Figure 3A. Reduced TEER values in experimentally treated monolayer cultures relative to baseline in vehicle-treated groups are indicative of compromised barrier functions, presumably due to the destruction of TJs.

To evaluate the effects of oxidative stress and altered HO1 activities on the barrier functions of ARPE19 monolayer cultures, ARPE19 cells were cultured on Transwell-like devices inserted into 24-well plates and were grown to full confluency according to Garcia-Ramirez et al.[68] To establish a baseline, TEER values were measured periodically for several days before the addition of experimental chemicals (not shown).

To assess the effect of HO1 inhibition, ZnPPIX was added to confluent ARPE19 cell monolayers, and TEER values were recorded at several time points over a 24-hour period

(Fig. 3B). Statistical analysis was carried out by ANOVA to compare the curves of ZnPPIX-treated versus vehicle-treated monolayer cultures. These analyses indicated that ZnPPIX exposure caused significant reductions in TEER values, implying loss of barrier functions. To determine if compromised barrier function was reversible, we replaced the ZnPPIX-containing media with ZnPPIX-free media and measured TEER values after medium replacement. Remarkably, electrical resistance recovered to normal values within several hours after ZnPPIX removal (Fig. 3B), suggesting that the loss of barrier functions was conditional on HO1 inhibition and was reversible when such inhibition had ended.

We also wondered if HO1 induction would protect ARPE19 barrier function under oxidative stress. Therefore, confluent ARPE19 cell cultures were treated with a combination of $NaIO_3$ and CoPP. The control cultures were treated with $NaIO_3$ alone or PBS. Over a 76-hour time frame, TEER values remained stable in PBS-treated cultures but decreased significantly in cultures treated with $NaIO_3$ alone (Fig. 3C). Notably, cultures treated with both $NaIO_3$ and CoPP maintained relatively stable TEER values (Fig. 3C). Overall, these data highlight the importance of HO1 in maintaining ARPE19 barrier function.

Defective RPE TJ Integrity in Global and RPE-Specific *Nrf2* Knockout Mice

Because of limitations associated with ARPE19 cultures, we complemented the in vitro studies by investigating RPE TJ stability in mice. In one set of experiments, we asked if mice deficient for NRF2 might display TJ phenotypes similar to those in NRF2-knockdown ARPE19 cell cultures. Due to the fact that $Nrf2^{-/-}$ mice suffer from RPE cell losses and develop choroidal neovascularization after 12 months of age,[35] we focused on younger stages in order to investigate RPE TJ phenotypes without being complicated by more advanced defects.

We examined RPE TJs in $Nrf2^{+/+}$ and $Nrf2^{-/-}$ mice by anti-ZO1 IF staining of RPE–choroid tissues (also referred to as "RPE tissues" for brevity). Choroid tissues were included merely for technical reasons, because it is impractical to remove choroid tissues without shattering the RPE monolayer. IF-stained RPE tissues were flatmounted with the RPE monolayer on top of the choroid tissues, and images were taken by fluorescence microscopy. Choroid tissues are invisible because of the specificity of anti-ZO1 staining and blockage of the light path by pigments in RPE cells.

At 2 months of age, anti-ZO1 IF staining patterns were indistinguishable between $Nrf2^{+/+}$ and $Nrf2^{-/-}$ mice, as both displayed strong and essentially continuous ZO1$^+$ signals along cell–cell junctions (Fig. 4A). By 4 months of age, ZO1$^+$ signals in $Nrf2^{+/+}$ mice remained strong and mostly continuous; however, $Nrf2^{-/-}$ mice exhibited numerous ZO1-negative gaps and weakly ZO1$^+$ intercellular junctions (Fig. 4B). ZO1$^+$ signals in RPE flatmounts were quantified similarly as described for ARPE19 cell cultures (Supplementary Fig. S2). Numerical data in Figures 4A and 4B confirm that, when the mice were 2 months of age, junctional ZO1 levels were similar between $Nrf2^{+/+}$ and $Nrf2^{-/-}$ mice, but at 4 months of age they were significantly reduced in the $Nrf2^{-/-}$ group.

To investigate whether NRF2 plays a cell-autonomous role in RPE cells in vivo, we generated RPE-specific, Dox-dependent *Nrf2* knockout mice by crossing floxed *Nrf2* mice with P_{VMD2}-*rtTA::tetO*-P_{bCMV}-*cre* (*VMD2-cre*) mice.[58,59] RPE specificity and the high efficiency of Dox-induced *VMD2-*

cre have been reported previously[59] but were also independently validated when we crossed *VMD2-cre* mice with a transgenic mouse line expressing Cre-dependent tdTomato reporter (Supplementary Fig. S3A).

In all experiments involving $Nrf2^{f/f}$/*VMD2-cre* mice, Cre expression was induced by feeding their mothers with Dox-supplemented chows, starting from the day a litter was born from $Nrf2^{f/f}$/*VMD2-cre* × $Nrf2^{f/f}$ breeding pairs and continuing for 3 weeks. In this procedure, $Nrf2^{f/f}$/*VMD2-cre* and $Nrf2^{f/f}$ neonatal mice were equally exposed to Dox. *Nrf2* deletion efficiency in RPE cells was determined by quantitative RT-PCR of total RNA purified from freshly isolated RPE cells. On average, *Nrf2* mRNA levels in Dox-treated $Nrf2^{f/f}$/*VMD2-cre* mice were only 20% of floxed controls (Supplementary Fig. S3B).

Phenotypic consequences of RPE-specific *Nrf2* deletion were analyzed by anti-ZO1 IF staining of RPE tissues, followed by flatmount imaging. At 4 months, no significant difference was observed between $Nrf2^{f/f}$ and $Nrf2^{f/f}$/*VMD2-cre* mice (Fig. 4C). At 8 months, however, $Nrf2^{f/f}$/*VMD2-cre* mice exhibited reduced ZO1 levels compared with $Nrf2^{f/f}$ mice (Fig. 4D). The delayed onset of TJ degeneration in $Nrf2^{f/f}$/*VMD2-cre* mice (Figs. 4C, 4D) relative to $Nrf2^{-/-}$ mice (Fig. 4B) was likely due to either or both of the following reasons: (1) although the *Nrf2* deletion efficiency in $Nrf2^{f/f}$/*VMD2-cre* mice was very high, it was nonetheless incomplete; and (2) *Nrf2* deletion in $Nrf2^{f/f}$/*VMD2-cre* mice is limited to RPE cells.

Partial NRF2 Dependence of HO1 Expression in Mice

To investigate whether HO1 expression in vivo was dependent on NRF2, we compared HO1 protein levels between $Nrf2^{+/+}$ and $Nrf2^{-/-}$ mice. Anti-HO1 IF staining of RPE tissues revealed that HO1 expression was reduced but not abolished in the RPE cells of $Nrf2^{-/-}$ mice (Fig. 5A). This result was validated by anti-HO1 Western blotting of isolated RPE tissues (Fig. 5B), indicating that anti-HO1 IF staining was a reliable method to quantify HO1 protein levels. Of note, these data are consistent with the in vitro data shown in Figure 2B, which demonstrate reduced HO1 expression in NRF2-knockdown ARPE19 cells.

Because HO1 expression in ARPE19 cells was upregulated under oxidative stress, we wondered if a similar phenomenon also exists in mice. Therefore, 2-month-old $Nrf2^{+/+}$ mice were injected with $NaIO_3$ intraperitoneally at a dosage previously shown not to directly cause RPE cell death in mice (10 mg/kg).[55–57] After 3 days, RPE tissues were subject to anti-HO1 IF staining, which revealed significantly higher HO1 levels in $NaIO_3$-treated $Nrf2^{+/+}$ mice than in PBS-injected controls (Fig. 5C, C1 vs. C3). Within the $Nrf2^{-/-}$ group, the $NaIO_3$-injected mice also had increased HO1 expression compared with the PBS-injected controls (Fig. 5C, C2 vs. C4). However, both $NaIO_3$- and PBS-injected $Nrf2^{-/-}$ mice had significantly lower HO1 levels than similarly treated $Nrf2^{+/+}$ mice (Fig. 5C, C1 vs. C2 and C3 vs. C4). These data led to a two-faceted conclusion: on the one hand, HO1 expression is dependent on NRF2; on the other hand, such dependence is incomplete, so that a certain level of HO1 still exists in $Nrf2^{-/-}$ mice.

In $Nrf2^{f/f}$/*VMD2-cre* mice, RPE-specific NRF2 deficiency significantly suppressed HO1 expression (Fig. 5D), suggesting that NRF2 promotes HO1 expression in RPE by cell autonomous mechanisms.
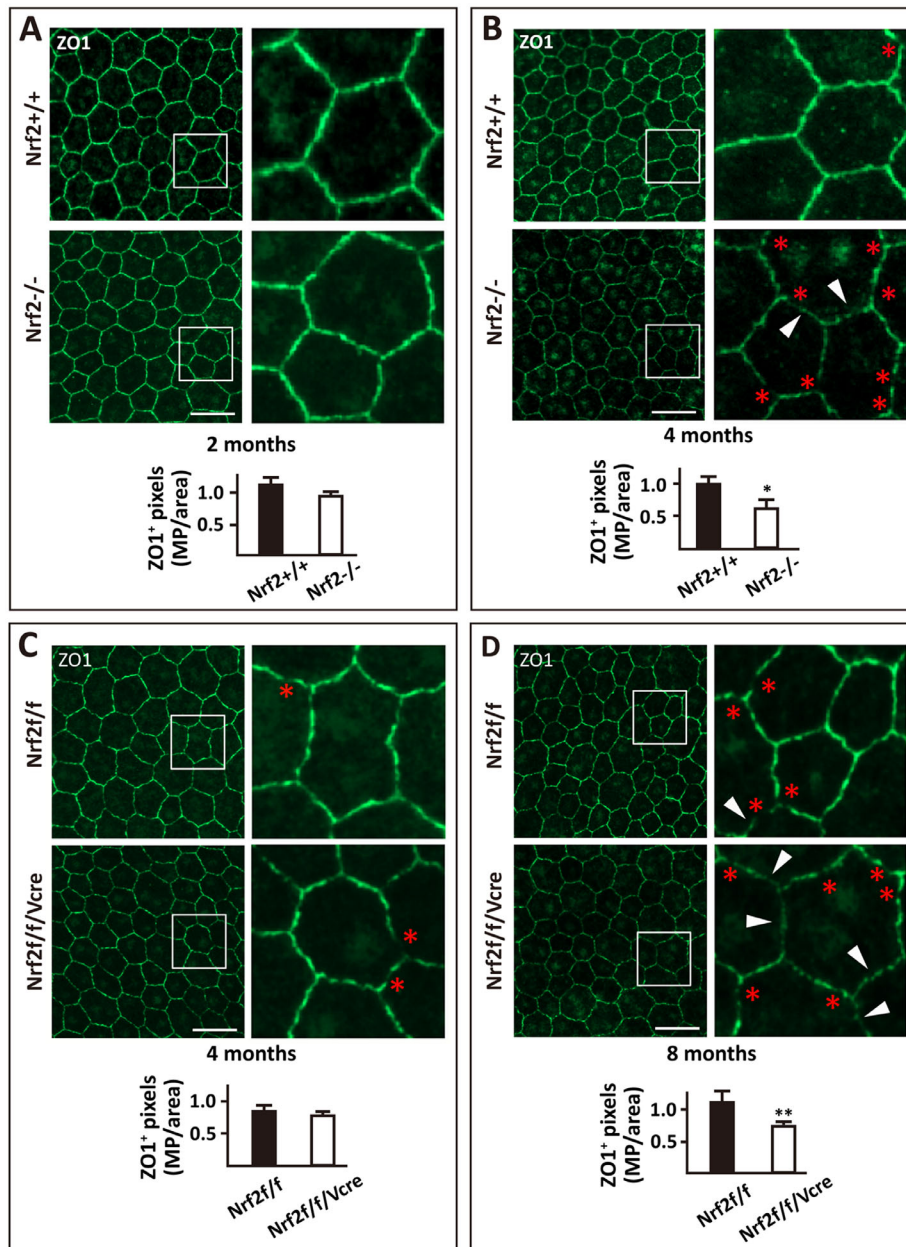
FIGURE 4. Role of NRF2 in RPE TJ integrity in mice. Wholemount RPE–choroid tissues were subject to anti-ZO1 IF staining, and then flatmounted with the RPE monolayer on top of the choroid. Images were taken by fluorescence microscopy. (**A, B**) $Nrf2^{+/+}$ and $Nrf2^{-/-}$ mice at 2 months (**A**) and 4 months (**B**) of age. (**C, D**) $Nrf2^{f/f}$ and $Nrf2^{f/f}/VMD2$-cre mice at 4 months (**C**) and 8 months (**D**) of age. For labeling, $VMD2$-cre is abbreviated as Vcre. Areas in *white boxes* are expanded to show details of the ZO1 staining patterns. *Red asterisks* indicate ZO1-negative regions at RPE cell junctions; *white arrowheads* point to weakly ZO1^{+} regions. *Scale bars*: 30 μm. ZO1^{+} pixels at the intercellular junctions were quantified after erasing the intracellular signals, as explained in Supplementary Figure S2. ZO1^{+} pixel values are presented as megapixels per 0.01-mm^2 area (MP/area); $n = 8$ mice. Statistical analyses were carried out using two-tailed Student's t-tests. *$P < 0.05$, **$P < 0.01$.

In Vivo Role of HO1 in the Structural Integrity of RPE TJs

We hypothesized that upregulated HO1 expression under oxidative stress might play a role in limiting the extent of RPE TJ damages. In order to test this hypothesis, we deemed it necessary to first validate that TJ structures are susceptible to destruction by low-dosage NaIO$_3$. Briefly, wild-type mice were injected intraperitoneally with NaIO$_3$ at 10 mg/kg, a dosage previously shown to be insufficient to cause RPE

cell death (10 mg/kg).[55–57] RPE tissues were analyzed by anti-ZO1 IF staining after 3 days. Results indicated that TJs were indeed moderately damaged by low-dosage injection of NaIO$_3$ (Fig. 6A).

Next, we tested whether such damages could be attenuated by CoPP. In this experiment, wild-type mice were first given intraperitoneal injections of NaIO$_3$, followed immediately by subretinal injections of CoPP in one eye and PBS in the contralateral eye. After 3 days, RPE tissues were isolated for anti-ZO1 IF staining, which indicated that RPE from
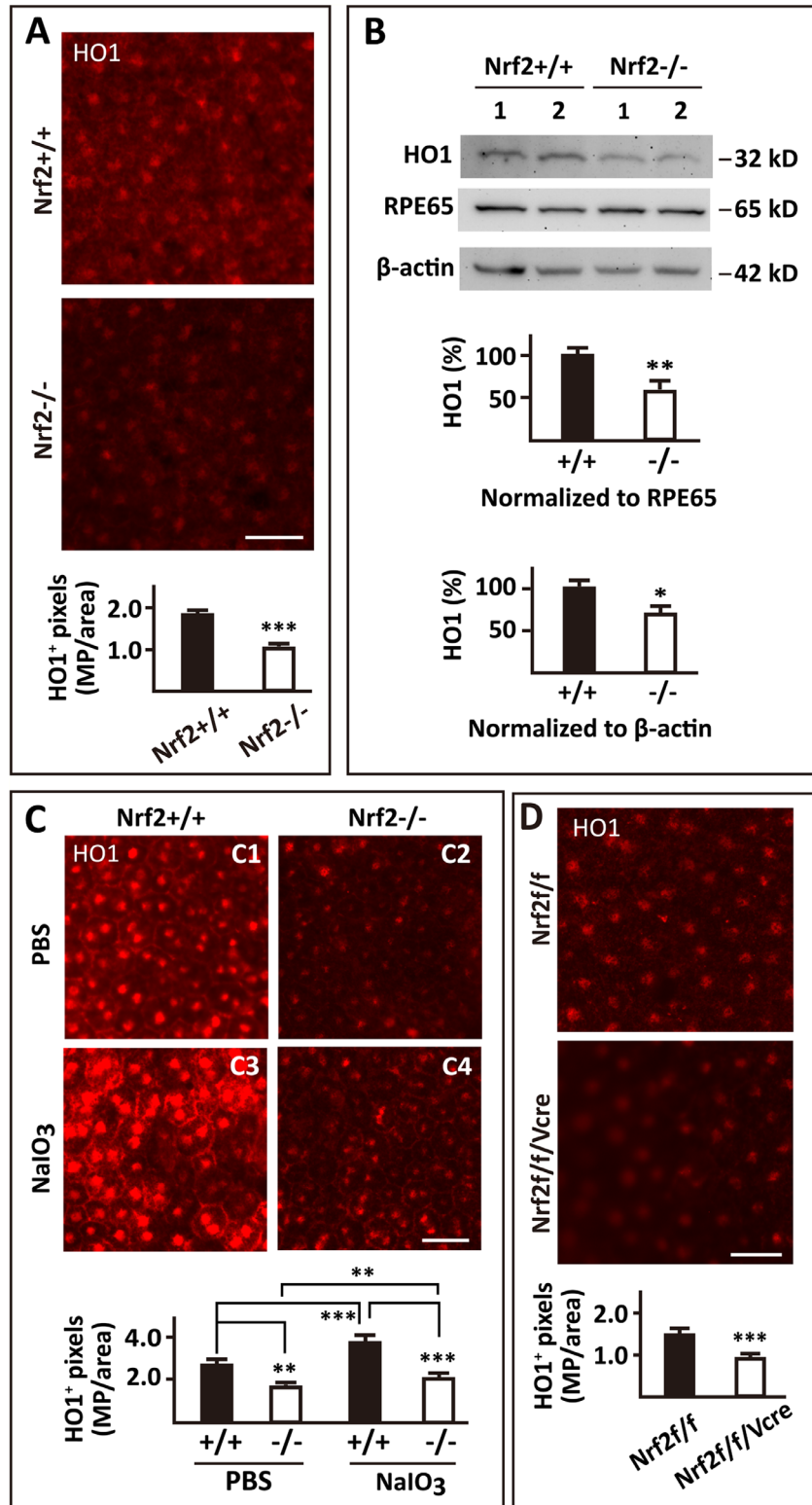
FIGURE 5. Partial NRF2 dependence of HO1 expression in RPE cells in mice. (**A**) Reduced NRF2 protein abundance in RPE cells of $Nrf2^{-/-}$ mice. Wholemount RPE tissues from 4-month-old $Nrf2^{+/+}$ and $Nrf2^{-/-}$ mice were subject to anti-HO1 IF staining followed by flatmount fluorescence microscopy. $HO1^+$ values are shown as megapixels per 0.01-mm² area (MP/area; applicable to the quantification of all other anti-HO1 stained images). (**B**) Anti-HO1 Western blot of RPE–choroid tissues from 2-month-old mice. RPE65 and β-actin were used for normalization. Normalized HO1 levels are shown as percentage of $Nrf2^{+/+}$ controls. (**C**) Upregulated HO1 expression under oxidative stress. Anti-HO1 IF staining of RPE tissues from 2-month-old $Nrf2^{+/+}$ and $Nrf2^{-/-}$ mice treated with $NaIO_3$ (10 mg/kg) or vehicle (PBS) by IP injection. After 3 days, stained RPE tissues were flatmounted and analyzed by fluorescence microscopy. (**D**) Reduced HO1 expression in $Nrf2^{f/f}/VMD2\text{-}cre$ mice. RPE tissues from 8-month-old $Nrf2^{f/f}$ and $Nrf2^{f/f}/VMD2\text{-}cre$ mice were analyzed by wholemount anti-HO1 IF staining followed by flatmount imaging. *Scale bars*: 30 μm; $n = 8$ mice (**A, C, D**) and $n = 6$ mice (**B**). Data were analyzed by two-tailed Student's t-tests. *$P < 0.05$, **$P < 0.01$, ***$P < 0.001$.
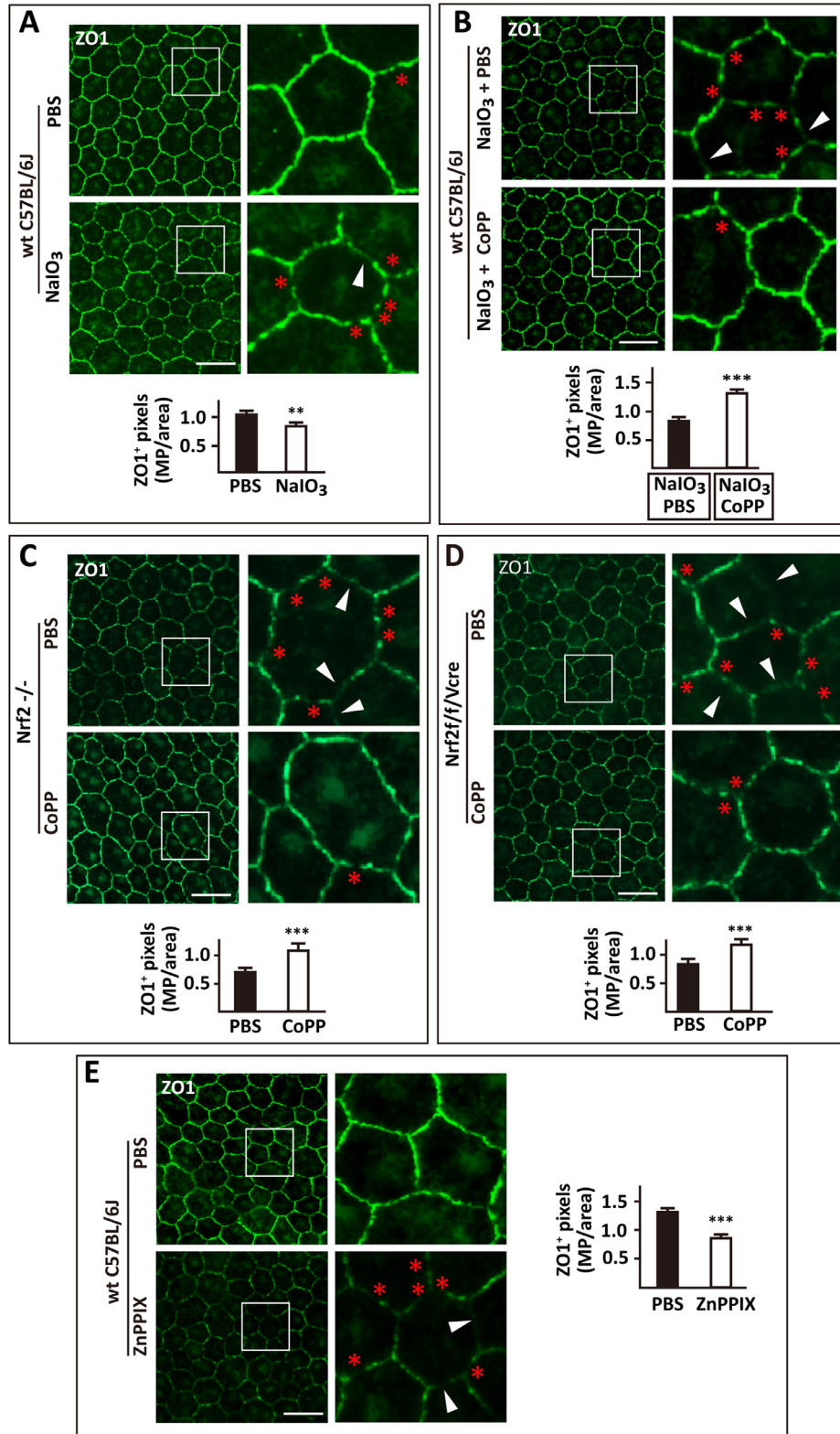
FIGURE 6. In vivo role of HO1 in protecting RPE TJs against oxidative stress. (**A**) Damage of RPE TJs by $NaIO_3$. Wild-type C57BL/6J mice (2 months old) were injected with a single dose of $NaIO_3$ (10 mg/kg IP) or vehicle (PBS). Three days later, RPE tissues were analyzed by anti-ZO1 IF staining. (**B**) Protection of RPE TJs against oxidant exposure by CoPP. Two-month-old wild-type C57BL/6J mice were injected with a single dose of $NaIO_3$ (10 mg/kg IP), 1 µL of 125-µM CoPP (subretinal in one eye), and 1 µL of PBS in the contralateral eye. Anti-ZO1 IF staining was performed after 3 days. (**C**) Protection of RPE TJs in $Nrf2^{-/-}$ mice by intraperitoneal injection of CoPP (1 mg/kg/dose, twice per week for 9 weeks, starting from 2 months of age). At the end of the injection regime, RPE tissues were analyzed by anti-ZO1 IF staining. (**D**) Rescue of RPE TJs in $Nrf2^{f/f}/VMD2-cre$ mice by CoPP. $Nrf2^{f/f}/VMD2-cre$ mice were treated with CoPP (1 mg/kg/dose) or

PBS by intraperitoneal injection twice per week for 4 months, starting from 4 months of age. RPE tissues were analyzed by anti-ZO1 IF staining at 8 months of age. (**E**) Destruction of RPE TJs by subretinal injection of the HO1 inhibitor ZnPPIX (125 µM, 1 µL/eye; 1 µL PBS for the contralateral eye). All expanded images correspond to the *white boxed areas* in the main images. ZO1 pixel values are presented as megapixels per 0.01-mm² area (MP/area). *Red asterisks* indicate ZO1-negative gaps along intercellular junctions; *white arrowheads* are pointed to long stretches of weak ZO1 staining signals. *Scale bars*: 30 µm; $n = 8$ mice. Data were evaluated by two-tailed Student's *t*-tests. **$P < 0.01$, ***$P < 0.001$.

CoPP-treated eyes had significantly stronger ZO1$^+$ signals (Fig. 6B). Therefore, HO1 activation by CoPP was highly effective in protecting RPE TJs against oxidative stress.

Because HO1 expression is not completely NRF2 dependent, we thought that CoPP might also protect RPE TJs in $Nrf2^{-/-}$ mice. Therefore, $Nrf2^{-/-}$ mice were injected with CoPP intraperitoneally twice a week for 2 months, starting from 2 months of age. At 4 months of age, RPE tissues were analyzed by anti-ZO1 IF staining, which demonstrated that junctional ZO1 levels were significantly higher in the CoPP-injected group (Fig. 6C).

In a similar experiment, $Nrf2^{f/f}/VMD2\text{-}cre$ mice were also subject to intraperitoneal CoPP injection, except that injections started from 4 months of age and ended at 8 month of age. Anti-ZO1 IF staining of RPE tissues revealed stronger junctional ZO1$^+$ signals in CoPP-injected $Nrf2^{f/f}/VMD2\text{-}cre$ mice than in PBS-injected controls (Fig. 6D).

To further determine if HO1 is indeed important for RPE TJs, we treated wild-type C57BL/6 mice by subretinal injection of ZnPPIX, a well-characterized HO1 inhibitor.[66,67] For controls, the contralateral eyes were injected with PBS. Three days after injection, RPE tissues were analyzed by anti-ZO1 IF staining. In ZnPPIX-injected eyes, RPE tissues displayed weak and discontinuous ZO1$^+$ signals, whereas RPE from PBS-injected eyes had strong and generally continuous ZO1$^+$ staining along intercellular junctions. Overall, these data indicate that HO1 protects TJ structures between RPE cells (Fig. 6E).

Increased RPE Permeability to Dextran Due to NRF2 Deficiency or Oxidant Exposure

RPE barrier function in mice was assessed by monitoring the diffusion of dextran (3 kD) across the RPE monolayer. The dextran molecules used in the study were conjugated with lysine so they could be cross-linked to tissue macromolecules during fixation with 4% PFA. Dextran was also biotinylated and hence detectable by staining with fluorophore-conjugated avidin (Supplementary Table S2). To begin the experiment, dextran solutions were injected into the systemic circulation through the retro-orbital sinus. After 15 minutes, mice were euthanized by perfusion, followed by 4% PFA for fixation. Eyes were enucleated, and frozen sections were prepared for avidin staining. The RPE monolayer in eye sections was identified as dark brown pigmented cells between the choroid and the photoreceptor layer of retinal tissues. The identity of RPE cells was also confirmed by anti-RPE65 IF staining of eye histological sections, visualized as RPE65$^+$ cells that were strongly pigmented and located between photoreceptors and the choroid (Supplementary Fig. S4).

To evaluate the role of NRF2 in RPE barrier function, we compared dextran diffusion through the RPE in 4-month-old $Nrf2^{+/+}$ and $Nrf2^{-/-}$ mice. In $Nrf2^{+/+}$ mice, dextran-positive signals were mostly stuck along the basal side of RPE cells, suggesting that the vast majority of dextran molecules were unable to cross the RPE barrier. In $Nrf2^{-/-}$ mice, however, dextran-positive signals were readily detectable further beyond the basal side, indicating that dextran molecules were in the process of diffusing through the RPE monolayer. Dextran-positive signals located away from the RPE basal side were quantified as megapixels per 1000-µm² area, and results confirmed significantly increased diffusion in $Nrf2^{-/-}$ mice (Fig. 7A).

Dextran distribution patterns were also compared between 8-month-old $Nrf2^{f/f}$ and $Nrf2^{f/f}/VMD2\text{-}cre$ mice. Similar to $Nrf2^{-/-}$ mice, the RPE in $Nrf2^{f/f}/VMD2\text{-}cre$ mice also displayed increased permeability to dextran (Fig. 7B).

The effect of oxidant exposure on RPE barrier function was also investigated. Wild-type C57BL/6J mice were injected with NaIO$_3$ or PBS intraperitoneally. Three days later, mice were subject to dextran diffusion analysis as described above. In PBS-injected mice, the majority of dextran-positive signals accumulated along the basal side of the RPE (Fig. 7C). In NaIO$_3$-injected mice, dextran-positive signals were abundantly present beyond the basal side (Fig. 7C).

On the other hand, most of the dextran molecules did not travel far enough to reach the photoreceptor region even in NRF2-deficient or NaIO$_3$-exposed mice. This outcome can be explained by the short time frame (15 minutes) between the dextran injection and euthanasia by perfusion. The rationale for choosing such a short time frame was that dextran molecules might diffuse too far away from the RPE after a longer time period, making it difficult to assess whether the dextran-positive signals originated from leaky RPE cells or retinal blood vessels.

RPE Barrier Function to Serum Albumin

RPE barrier function to endogenous serum albumin was evaluated by quantifying the amount of mouse albumin that had passed through the RPE and deposited on retinal tissues. We focused on a narrow region of retinal tissues at the junction between the RPE and photoreceptors (PRs). Because the PR tissues are avascular, focusing on this narrow region maximizes the chance that the observed albumin-positive signals may indeed reflect RPE permeability rather than retinal vascular leakage.

To deplete circulating albumin, mice were euthanized by perfusion with PBS, and tissues were fixed by the infusion of 4% PFA. Eyes were isolated, and frozen sections were prepared for anti-mouse albumin IF staining. Albumin-positive signals at the RPE–PR junction were quantified as megapixels per area of 1000 µm² (Fig. 8).

Both global and RPE-specific $Nrf2$ knockout mice were analyzed. When 4-month-old $Nrf2^{+/+}$ and $Nrf2^{-/-}$ mice were examined, significantly higher levels of albumin were found in $Nrf2^{-/-}$ mice than in $Nrf2^{+/+}$ controls (Fig. 8A). $Nrf2^{f/f}$ and $Nrf2^{f/f}/VMD2\text{-}cre$ mice were analyzed at 8 months of age, which revealed elevated albumin levels in $Nrf2^{f/f}/VMD2\text{-}cre$ mice compared to floxed controls (Fig. 8B).
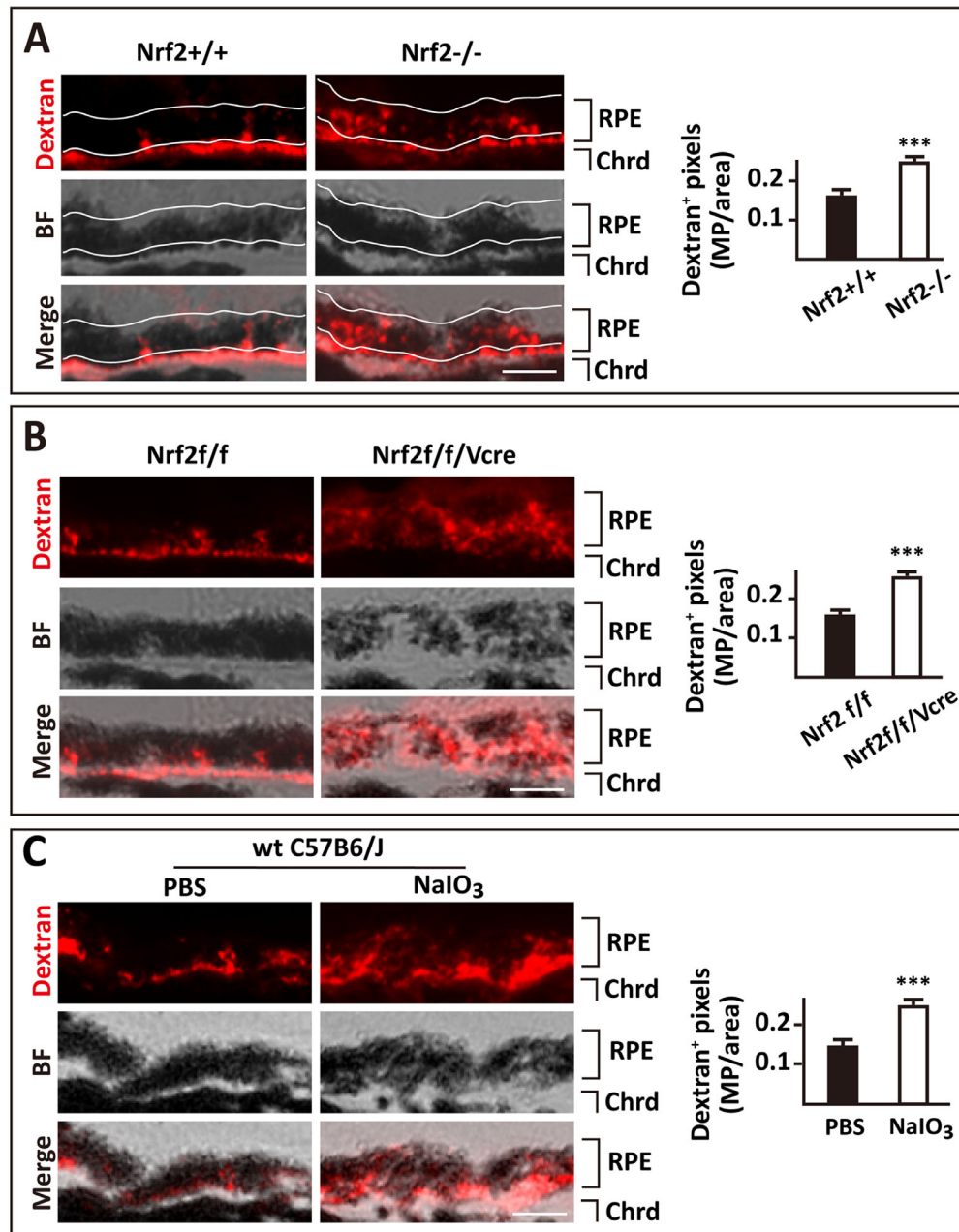
Figure 7. Increased RPE permeability to dextran due to NRF2 deficiency or oxidant exposure. (**A**) Increased RPE permeability to dextran (3 kD) in *Nrf2*$^{-/-}$ mice. Four-month-old *Nrf2*$^{+/+}$ and *Nrf2*$^{-/-}$ mice were injected with biotinylated, lysine-conjugated dextran (5 mg/kg) through the retro-orbital sinus and were perfused with PBS after 15 minutes. Tissues were fixed by infusion of 4% PFA. Frozen sections of eyes were prepared, and dextran distribution was monitored by staining with Alexa Fluor 549 avidin (Supplementary Table S2). The *curvy white lines* mark the area of RPE cells above the basal side. RPE cells were identified in the brightfield (BF) as strongly pigmented cells separated from choroid (Chrd) tissues (also pigmented) by a narrow, non-pigmented tissue consisting of choroid capillaries and the Bruch's membrane (not labeled). The identity of RPE cells was also confirmed by anti-RPE65 IF staining (Supplementary Fig. S4). Dextran-positive signals between the two *white lines* were quantified as megapixels per area of 1000 µm² (MP/area). (**B**) Increased RPE permeability to dextran in *Nrf2*$^{f/f}$/*VMD2-cre* mice. Both *Nrf2*$^{f/f}$ and *Nrf2*$^{f/f}$/*VMD2-cre* mice were 8 months old. (**C**) Increased RPE permeability to dextran in 2-month-old wild-type mice injected with NaIO$_3$ (10 mg/kg IP). Mice were euthanized for analysis 3 days after injection. *Scale bars*: 10 µm; $n = 8$ mice. Data were analyzed by two-tailed Student's *t*-tests. ***$P < 0.001$.

We also investigated whether HO1 activation by CoPP could rescue RPE barrier functions in *Nrf2*$^{-/-}$ mice. Because the loss of RPE TJs became detectable in *Nrf2*$^{-/-}$ mice at 4 months of age but not at 2 months, we started intraperitoneal injections of CoPP (or PBS as vehicle) in 2-month-old *Nrf2*$^{-/-}$ mice, which continued twice a week until 4 months of age. Anti-mouse albumin IF staining on eye sections demonstrated significantly lower amounts of albumin in CoPP-injected *Nrf2*$^{-/-}$ mice than in PBS-injected controls (Fig. 8C), suggesting that HO1 activation by CoPP indeed rescued RPE barrier function.
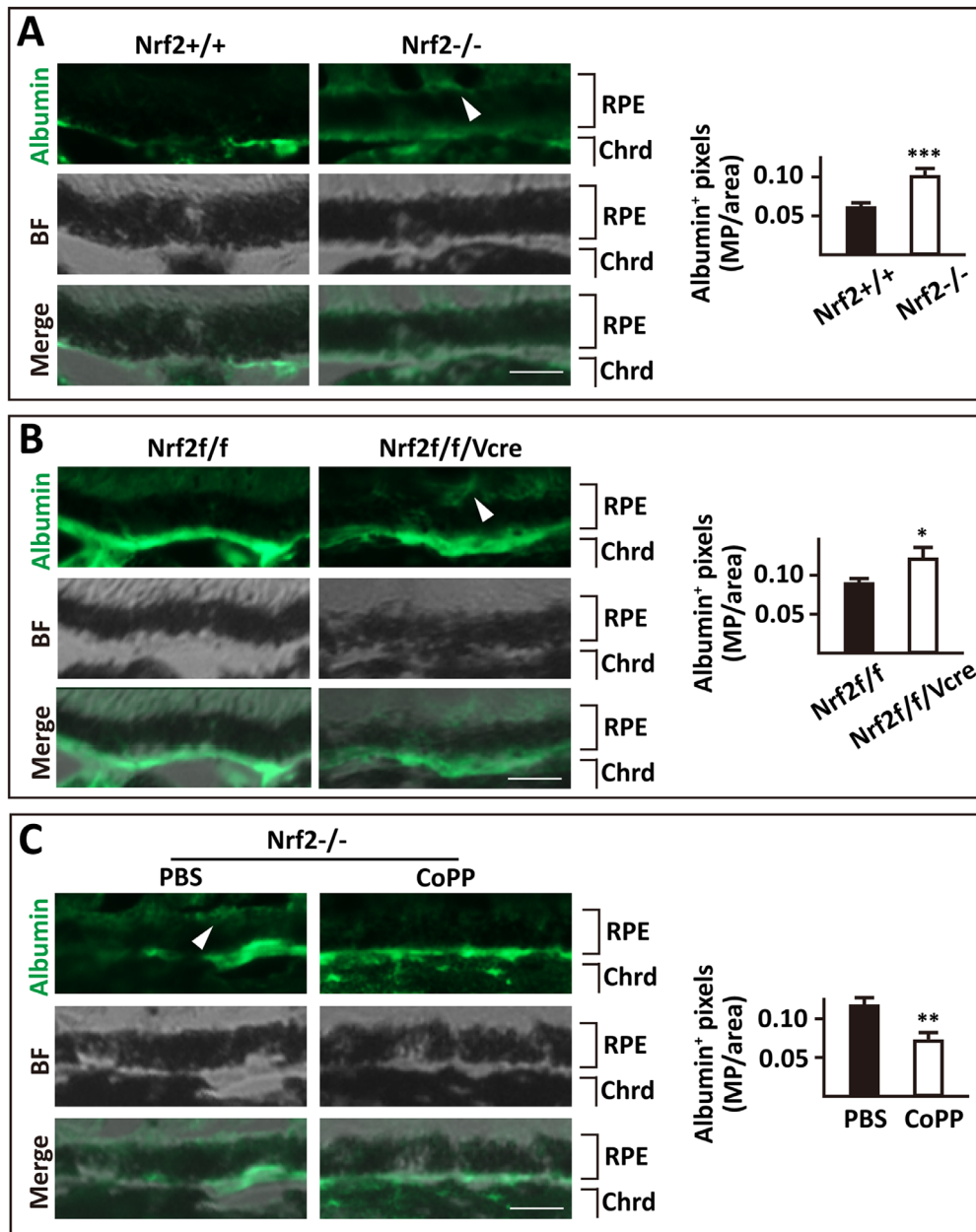
FIGURE 8. Analyses of RPE permeability to endogenous serum albumin. (**A**) Increased RPE permeability to endogenous albumin in $Nrf2^{-/-}$ mice. Four-month-old $Nrf2^{+/+}$ and $Nrf2^{-/-}$ mice were perfused with PBS and fixed with 4% PFA. Frozen eye sections were analyzed by anti-albumin IF staining. Note the stronger staining signal in $Nrf2^{-/-}$ mice in the area near the apical side of the RPE (*white arrowhead*). Albumin-positive pixel values are shown as megapixels per 1000-μm^2 area (MP/area). BF, brightfield; Chrd, choiroid. (**B**) Increased RPE permeability to endogenous albumin in $Nrf2^{f/f}$/VMD2-cre mice. $Nrf2^{f/f}$ and $Nrf2^{f/f}$/VMD2-cre mice were euthanized by perfusion at 8 months of age. Anti-albumin IF staining of frozen eye sections revealed stronger staining in $Nrf2^{f/f}$/VMD2-cre mice (*white arrowhead*) than in floxed controls. (**C**) Protection of RPE barrier function in $Nrf2^{-/-}$ mice by CoPP. $Nrf2^{-/-}$ mice were injected intraperitoneally with CoPP at 1 mg/kg/dose, twice a week for 9 weeks, starting from 2 months of age. PBS was injected as vehicle. At 4 months of age, mice were euthanized by perfusion and analyzed by anti-albumin IF staining of frozen eye sections. Although albumin-positive signals remained elevated in PBS-injected mice (*white arrowhead*), they became very faint in CoPP-injected $Nrf2^{-/-}$ mice. *Scale bars*: 10 μm. Data were analyzed by two-tailed Student's *t*-tests; $n = 8$ mice. *$P < 0.05$, **$P < 0.01$, ***$P < 0.001$.

Destructive Effects of Heme on RPE Integrity

Because HO1 plays a major role in heme degradation, we asked whether excess heme might cause deterioration of RPE TJs. To address this issue, we directly treated ARPE19 cells with hemin (a heme precursor), and found that junctional ZO1 levels were indeed reduced in hemin-treated cultures (Fig. 9A). Reduced ZO1 levels were not due to ARPE19 cell death, because hemin-treated ARPE19 cells had normal viability (Supplementary Fig. S5). Next, we investi-
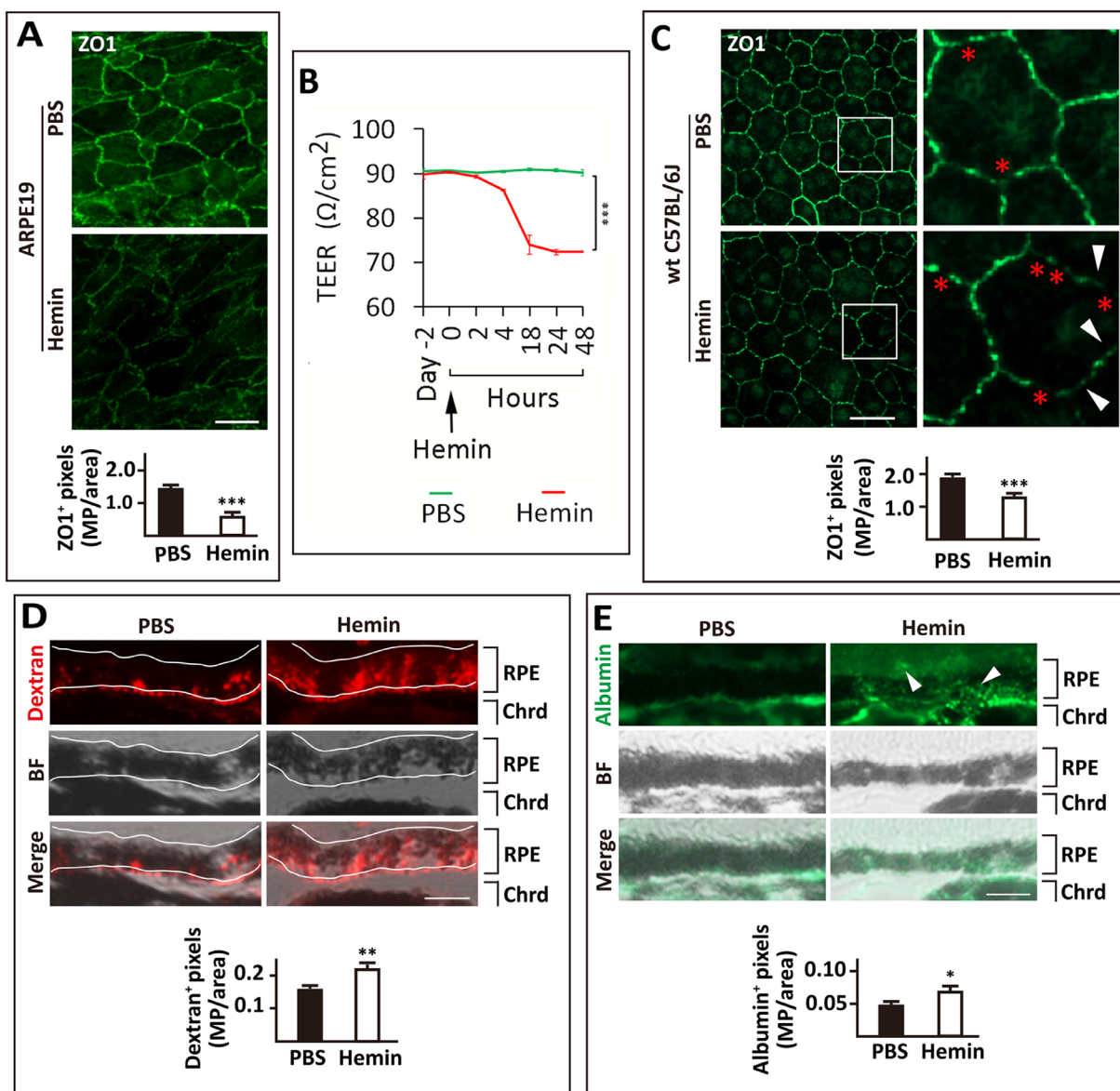
FIGURE 9. Destructive effects of hemin treatment on RPE TJ integrity and barrier function. (**A**) Anti-ZO1 IF staining of ARPE19 cells after hemin treatment (0.5 µM, 16 hours). (**B**) Destruction of ARPE19 barrier functions by hemin. Confluent ARPE19 cell cultures were supplemented with hemin (0.5 µM), and TEER values were recorded at the indicated time points. (**C**) Anti-ZO1 IF staining of RPE tissues from wild-type mice injected with hemin (1 mg/kg/dose) or PBS by intraperitoneal injection, twice per week for 3 months, starting from 2 months of age. In **A** and **C**, MP/area indicates megapixels per 0.01-mm² area. (**D**, **E**) Alexa Fluor 549 avidin (**D**) and anti-albumin (**E**) staining of frozen eye sections, prepared from hemin- or PBS-treated wild-type C57BL/6J mice. Biotin–dextran injection was carried out through the retro-orbital sinus, and mice were euthanized by perfusion after 15 minutes. Dextran-positive and albumin-positive signals were quantified as megapixels per area of 1000 µm² (MP/area). BF, brightfield. *Scale bars*: 30 µm (**A, C**); 10 µm (**D, E**). In **A, C, D**, and **E**, $n = 8$ mice, and the data were analyzed by two-tailed Student's *t*-tests. In **B**, $n = 3$ mice, and the data were analyzed by two-way ANOVA tests. *$P < 0.05$, **$P < 0.01$, ***$P < 0.001$.

gated if barrier function in ARPE19 monolayer cultures was compromised by hemin treatment. As shown in Figure 9B, hemin rapidly and dramatically reduced TEER values. Taken together, these data suggest that heme is harmful to ARPE19 barrier functions.

To extend this study to mice, we injected hemin into wild-type C57BL/6J mice intraperitoneally. Anti-ZO1 IF staining of RPE tissues demonstrated that junctional ZO1 levels were significantly reduced in hemin-treated mice relative to PBS-

injected controls (Fig. 9C). To evaluate dextran diffusion, hemin- or PBS-injected wild-type mice were injected with biotinylated dextran through retro-orbital sinus. Frozen eye sections were stained with Alexa Fluor 549 avidin, which revealed that diffusion of dextran was significantly increased in the hemin-treated mice (Fig. 9D). RPE permeability was also analyzed by anti-albumin IF staining on eye sections. At the RPE–PR junction, albumin contents were significantly higher in the hemin-treated mice than in PBS-treated mice

(Fig. 9E). Overall, these data suggest that heme is a significant contributor to the deterioration of RPE TJ and barrier functions.

DISCUSSION

Despite the general understanding that RPE barrier functions are prone to damages by oxidative stress, there is little knowledge on how TJ structural integrity per se is affected by oxidative stress, especially in vivo. This situation stems from the fact that severe oxidant exposure of RPE cells typically leads to widespread cell death, making it difficult to determine whether TJ disassembly is a primary consequence of oxidative stress or part of the cell death process.

Normal TJs consist of at least three different types of proteins: (1) transmembrane proteins such as occludins (OCLNs) and claudins (CLDN), which tightly interlock with each other from opposing cell membranes; (2) adaptor proteins such as dimers or heterodimers of ZO1, ZO2, and ZO3, which associate with both the intracellular regions of OCLNs/CLDNs and cytoskeletal actin; and (3) cytoskeletal actin filaments, which secure the TJ complexes.[1,69]

A reliable indicator of intact TJ structures is the localization of ZO1 at intercellular junctions. In this study, we showed that TJ structures in RPE cells are sensitive to oxidative stress, which was demonstrated at the structural level by the loss of junctional ZO1 and at the functional level by increased RPE permeability to dextran and serum albumin. These findings were made both in cultured RPE cells and in mice. Furthermore, the NRF2–HO1 pathway had protective effects for TJ structures and RPE barrier function. Data from RPE cell–specific Nrf2 knockout mice also demonstrate that NRF2 is protective from within RPE cells in a cell autonomous manner. On the other hand, our data do not rule out the possibility that NRF2 in other cell types might also indirectly contribute to RPE integrity through regulation of systemic redox balance. These two possibilities are not mutually exclusive.

An interesting phenomenon is that NRF2 levels are upregulated under oxidative stress, presumably as an adaptive response (Fig. 1B). In turn, upregulated NRF2 activates antioxidant mechanisms by transcriptional upregulation of its target genes. HMOX1, a NRF2 target gene encoding HO1, is also upregulated under oxidative stress, essentially in parallel to NRF2 (Figs. 1B, 2A). Our data demonstrate a cause and effect relationships between Nrf2 expression and HO1 upregulation under oxidative stress. NRF2 knockdown in vitro or NRF2 deficiency in vivo both prevented HO1 upregulation by $NaIO_3$ (Figs. 2C, 5C). At the functional level, there is also a cause-and-effect relationship between NRF2 expression and maintenance of TJ integrity, with NRF2 deficiency leading to TJ disintegration and loss of RPE barrier function (Figs. 1D, 4, 7, 8). Likewise, a similar relationship can also be proposed for HO1 and TJ integrity. The HO1 inducer CoPP promotes TJ integrity and RPE barrier function (Figs. 2F, 3, 9), whereas HO1 knockdown or treatment with HO1 inhibitor (ZnPPIX) has the opposite effect.

Mechanistically, HO1 exerts its antioxidant functions by catalyzing heme degradation, because heme supports ROS production but heme degradation products biliverdin and CO are antioxidants.[43–46] Therefore, activation of the NRF2–HO1 axis may mitigate, although not enough to completely abolish, the damaging effects of oxidative stress on RPE TJs. In support of this mechanism, exogenous heme added to ARPE19 cell cultures or injected into mice caused TJ disassembly and RPE barrier breaching (Fig. 9).

NRF2 also exerts its antioxidant functions by upregulating other antioxidant enzymes besides HO1, notably superoxide dismutase (SOD)1 and SOD2, which also play important roles in the retina and RPE cells.[30,39,70,71] Although a deficiency in these proteins has been reported to cause RPE cell loss or choroidal neovascularization, their direct roles in TJ structural organization have not been reported.[25,39] Importantly, because we were able to rescue TJ integrity in Nrf2 knockout mice or NRF2 knockdown ARPE19 cells with CoPP, it seems that, in our experimental system, HMOX1 (HO1) is the predominant NRF2 target critically required for TJ stability in RPE cells.

In several cultured cell lines, such as bovine aortic endothelial cells,[72] colon tissue epithelial cells,[73] and renal tubular epithelial cells,[74] exposure to ROS-generating compounds such as $NaIO_3$ is known to cause the disassembly of TJs. However, a literature search found no in vivo studies investigating how TJ integrity in any cell type is affected by dynamic interactions between oxidative stress and antioxidant mechanisms. Therefore, the implications of the findings made in this study might go beyond RPE cells.

We also believe that this study may have significant relevance to human AMD pathogenesis. Oxidative stress is a common condition in humans and is typically associated with oxidative metabolism, light exposure, and, in some cases, direct exposure to oxidants such as smoking products. Chronic oxidative stress in RPE cells may lead to breaching of the RPE barrier, which is an early event in AMD progression. The importance of the NRF2–HO1 pathway in humans is highlighted by the association of several polymorphism alleles in the NRF2 and HMOX1 loci with increased incidence of AMD.[75,76] Therefore, understanding the roles of the NRF2–HO1 pathway in mouse RPE may provide insights that are highly relevant to AMD pathogenesis in humans.

References

1. Lakkaraju A, Umapathy A, Tan LX, et al. The cell biology of the retinal pigment epithelium [published online ahead of print February 24, 2020]. Prog Retin Eye Res, https://doi.org/10.1016/j.preteyeres.2020.100846.

2. Booij JC, Baas DC, Beisekeeva J, Gorgels TG, Bergen AA. The dynamic nature of Bruch's membrane. Prog Retin Eye Res. 2010;29:1–18.

3. Murali A, Krishnakumar S, Subramanian A, Parameswaran S. Bruch's membrane pathology: a mechanistic perspective. Eur J Ophthalmol. 2020;30:1195–1206.

4. Tsukita S, Furuse M, Itoh M. Multifunctional strands in tight junctions. Nat Rev Mol Cell Biol. 2001;2:285–293.

5. Bird A. Role of retinal pigment epithelium in age-related macular disease: a systematic review. Br J Ophthalmol. 2021;105:1469–1474.

6. Fields MA, Del Priore LV, Adelman RA, Rizzolo LJ. Interactions of the choroid, Bruch's membrane, retinal pigment epithelium, and neurosensory retina collaborate

to form the outer blood-retinal-barrier. *Prog Retin Eye Res.* 2020;76:100803.

7. Benedicto I, Lehmann GL, Ginsberg M, et al. Concerted regulation of retinal pigment epithelium basement membrane and barrier function by angiocrine factors. *Nat Commun.* 2017;8:15374.

8. Georgiadis A, Tschernutter M, Bainbridge JW, et al. The tight junction associated signalling proteins ZO-1 and ZONAB regulate retinal pigment epithelium homeostasis in mice. *PLoS One.* 2010;5:e15730.

9. Miller SS, Steinberg RH. Active transport of ions across frog retinal pigment epithelium. *Exp Eye Res.* 1977;25:235–248.

10. Sivakami S, Ganapathy V, Leibach FH, Miyamoto Y. The gamma-aminobutyric acid transporter and its interaction with taurine in the apical membrane of the bovine retinal pigment epithelium. *Biochem J.* 1992;283:391–397.

11. Nolan ND, Jenny LA, Wang NK, Tsang SH. Retinal pigment epithelium lipid metabolic demands and therapeutic restoration. *Taiwan J Ophthalmol.* 2021;11:216–220.

12. Young RW, Bok D. Participation of the retinal pigment epithelium in the rod outer segment renewal process. *J Cell Biol.* 1969;42:392–403.

13. LaVail MM. Rod outer segment disk shedding in rat retina: relationship to cyclic lighting. *Science.* 1976;194:1071–1074.

14. Storm T, Burgoyne T, Futter CE. Membrane trafficking in the retinal pigment epithelium at a glance. *J Cell Sci.* 2020;133:jcs238279.

15. Yoshinaga A, Kajihara N, Kukidome D, et al. Hypoglycemia induces mitochondrial reactive oxygen species production through increased fatty acid oxidation and promotes retinal vascular permeability in diabetic mice. *Antioxid Redox Signal.* 2021;34:1245–1259.

16. Chen Q, Tang L, Xin G, et al. Oxidative stress mediated by lipid metabolism contributes to high glucose-induced senescence in retinal pigment epithelium. *Free Radic Biol Med.* 2019;130:48–58.

17. Kajihara N, Kukidome D, Sada K, et al. Low glucose induces mitochondrial reactive oxygen species via fatty acid oxidation in bovine aortic endothelial cells. *J Diabetes Investig.* 2017;8:750–761.

18. Kunchithapautham K, Atkinson C, Rohrer B. Smoke exposure causes endoplasmic reticulum stress and lipid accumulation in retinal pigment epithelium through oxidative stress and complement activation. *J Biol Chem.* 2014;289:14534–14546.

19. Neal SE, Buehne KL, Besley NA, et al. Resveratrol protects against hydroquinone-induced oxidative threat in retinal pigment epithelial cells. *Invest Ophthalmol Vis Sci.* 2020;61:32.

20. Ozkaya EK, Anderson G, Dhillon B, Bagnaninchi PO. Blue-light induced breakdown of barrier function on human retinal epithelial cells is mediated by PKC-ζ over-activation and oxidative stress. *Exp Eye Res.* 2019;189:107817.

21. Zhang M, Jiang N, Chu Y, et al. Dysregulated metabolic pathways in age-related macular degeneration. *Sci Rep.* 2020;10:2464.

22. Gu X, Neric NJ, Crabb JS, et al. Age-related changes in the retinal pigment epithelium (RPE). *PLoS One.* 2012;7:e38673.

23. Sachdeva MM, Cano M, Handa JT. Nrf2 signaling is impaired in the aging RPE given an oxidative insult. *Exp Eye Res.* 2014;119:111–114.

24. Bonilha VL, Bell BA, Rayborn ME, et al. Absence of DJ-1 causes age-related retinal abnormalities in association with increased oxidative stress. *Free Radic Biol Med.* 2017;104:226–237.

25. Mao H, Seo SJ, Biswal MR, et al. Mitochondrial oxidative stress in the retinal pigment epithelium leads to localized retinal degeneration. *Invest Ophthalmol Vis Sci.* 2014;55:4613–4627.

26. Hua J, Chen H, Chen Y, et al. MITF acts as an anti-oxidant transcription factor to regulate mitochondrial biogenesis and redox signaling in retinal pigment epithelial cells. *Exp Eye Res.* 2018;170:138–147.

27. Jadeja RN, Jones MA, Abdelrahman AA, et al. Inhibiting microRNA-144 potentiates Nrf2-dependent antioxidant signaling in RPE and protects against oxidative stress-induced outer retinal degeneration. *Redox Biol.* 2020;28:101336.

28. Xu XZ, Tang Y, Cheng LB, et al. Targeting Keap1 by miR-626 protects retinal pigment epithelium cells from oxidative injury by activating Nrf2 signaling. *Free Radic Biol Med.* 2019;143:387–396.

29. Wang K, Zheng M, Lester KL, Han Z. Light-induced Nrf2$^{-/-}$ mice as atrophic age-related macular degeneration model and treatment with nanoceria laden injectable hydrogel. *Sci Rep.* 2019;9:14573.

30. Brown EE, DeWeerd AJ, Ildefonso CJ, Lewin AS, Ash JD. Mitochondrial oxidative stress in the retinal pigment epithelium (RPE) led to metabolic dysfunction in both the RPE and retinal photoreceptors. *Redox Biol.* 2019;24:101201.

31. Tonelli C, Chio IIC, Tuveson DA. Transcriptional regulation by Nrf2. *Antioxid Redox Signal.* 2018;29:1727–1745.

32. Chan K, Lu R, Chang JC, Kan YW. NRF2, a member of the NFE2 family of transcription factors, is not essential for murine erythropoiesis, growth, and development. *Proc Natl Acad Sci USA.* 1996;93:13943–13948.

33. Rowan S, Jiang S, Francisco SG, et al. Aged Nrf2-null mice develop all major types of age-related cataracts. *Invest Ophthalmol Vis Sci.* 2021;62:10.

34. Osburn WO, Kensler TW. Nrf2 signaling: an adaptive response pathway for protection against environmental toxic insults. *Mutat Res.* 2008;659:31–39.

35. Zhao Z, Chen Y, Wang J, et al. Age-related retinopathy in NRF2-deficient mice. *PLoS One.* 2011;6:e19456.

36. Liang C, Xue Z, Cang J, Wang H, Li P. Dimethyl sulfoxide induces heme oxygenase-1 expression via JNKs and Nrf2 pathways in human umbilical vein endothelial cells. *Mol Cell Biochem.* 2011;355:109–115.

37. Chen CY, Jang JH, Li MH, Surh YJ. Resveratrol upregulates heme oxygenase-1 expression via activation of NF-E2-related factor 2 in PC12 cells. *Biochem Biophys Res Commun.* 2005;331:993–1000.

38. Chen XL, Varner SE, Rao AS, et al. Laminar flow induction of antioxidant response element-mediated genes in endothelial cells. A novel anti-inflammatory mechanism. *J Biol Chem.* 2003;278:703–711.

39. Imamura Y, Noda S, Hashizume K, et al. Drusen, choroidal neovascularization, and retinal pigment epithelium dysfunction in SOD1-deficient mice: a model of age-related macular degeneration. *Proc Natl Acad Sci USA.* 2006;103:11282–11287.

40. Liu Y, Ortiz de Montellano PR. Reaction intermediates and single turnover rate constants for the oxidation of heme by human heme oxygenase-1. *J Biol Chem.* 2000;275:5297–5307.

41. Tenhunen R, Marver HS, Schmid R. The enzymatic conversion of heme to bilirubin by microsomal heme oxygenase. *Proc Natl Acad Sci USA.* 1968;61:748–755.

42. Sugishima M, Sakamoto H, Higashimoto Y, Noguchi M, Fukuyama K. Crystal structure of rat heme oxygenase-1 in complex with biliverdin-iron chelate. Conformational change of the distal helix during the heme cleavage reaction. *J Biol Chem.* 2003;278:32352–32358.

43. Porto BN, Alves LS, Fernandez PL, et al. Heme induces neutrophil migration and reactive oxygen species

generation through signaling pathways characteristic of chemotactic receptors. *J Biol Chem*. 2007;282:24430–24436.

44. Matsumoto H, Ishikawa K, Itabe H, Maruyama Y. Carbon monoxide and bilirubin from heme oxygenase-1 suppresses reactive oxygen species generation and plasminogen activator inhibitor-1 induction. *Mol Cell Biochem*. 2006;291:21–28.

45. Morita T. Heme oxygenase and atherosclerosis. *Arterioscler Thromb Vasc Biol*. 2005;25:1786–1795.

46. Barcellos-de-Souza P, Moraes JA, de-Freitas-Junior JC, Morgado-Diaz JA, Barja-Fidalgo C, Arruda MA. Heme modulates intestinal epithelial cell activation: involvement of NADPHox-derived ROS signaling. *Am J Physiol Cell Physiol*. 2013;304:C170–C179.

47. Saito Y, Kuse Y, Inoue Y, Nakamura S, Hara H, Shimazawa M. Transient acceleration of autophagic degradation by pharmacological Nrf2 activation is important for retinal pigment epithelium cell survival. *Redox Biol*. 2018;19:354–363.

48. Tang Z, Ju Y, Dai X, et al. HO-1-mediated ferroptosis as a target for protection against retinal pigment epithelium degeneration. *Redox Biol*. 2021;43:101971.

49. Woo JM, Shin DY, Lee SJ, et al. Curcumin protects retinal pigment epithelial cells against oxidative stress via induction of heme oxygenase-1 expression and reduction of reactive oxygen. *Mol Vis*. 2012;18:901–908.

50. Poss KD, Tonegawa S. Heme oxygenase 1 is required for mammalian iron reutilization. *Proc Natl Acad Sci USA*. 1997;94:10919–10924.

51. Subramanian P, Mendez EF, Becerra SP. A novel inhibitor of 5-lipoxygenase (5-LOX) prevents oxidative stress-induced cell death of retinal pigment epithelium (RPE) cells. *Invest Ophthalmol Vis Sci*. 2016;57:4581–4588.

52. Han D, Wu X, Liu L, Shu W, Huang Z. Sodium tanshinone IIA sulfonate protects ARPE-19 cells against oxidative stress by inhibiting autophagy and apoptosis. *Sci Rep*. 2018;8:15137.

53. Mulfaul K, Ozaki E, Fernando N, et al. Toll-like receptor 2 facilitates oxidative damage-induced retinal degeneration. *Cell Rep*. 2020;30:2209–2224.e5.

54. Liu X, Ward K, Xavier C, et al. The novel triterpenoid RTA 408 protects human retinal pigment epithelial cells against H_2O_2-induced cell injury via NF-E2-related factor 2 (Nrf2) activation. *Redox Biol*. 2016;8:98–109.

55. Zhang N, Zhang X, Girardot PE, et al. Electrophysiologic and morphologic strain differences in a low-dose $NaIO_3$-induced retinal pigment epithelium damage model. *Transl Vis Sci Technol*. 2021;10:10.

56. Moriguchi M, Nakamura S, Inoue Y, et al. Irreversible photoreceptors and RPE cells damage by intravenous sodium iodate in mice is related to macrophage accumulation. *Invest Ophthalmol Vis Sci*. 2018;59:3476–3487.

57. Wang J, Iacovelli J, Spencer C, Saint-Geniez M. Direct effect of sodium iodate on neurosensory retina. *Invest Ophthalmol Vis Sci*. 2014;55:1941–1953.

58. Xue P, Hou Y, Chen Y, et al. Adipose deficiency of Nrf2 in ob/ob mice results in severe metabolic syndrome. *Diabetes*. 2013;62:845–854.

59. Le YZ, Zheng W, Rao PC, et al. Inducible expression of cre recombinase in the retinal pigmented epithelium. *Invest Ophthalmol Vis Sci*. 2008;49:1248–1253.

60. Shen J, He J, Wang F. Isolation and culture of primary mouse retinal pigment epithelial (RPE) cells with Rho-kinase and TGFβR-1/ALK5 inhibitor. *Med Sci Monit*. 2017;23:6132–6136.

61. Dunn KC, Aotaki-Keen AE, Putkey FR, Hjelmeland LM. ARPE-19, a human retinal pigment epithelial cell line with differentiated properties. *Exp Eye Res*. 1996;62:155–169.

62. Reichard JF, Motz GT, Puga A. Heme oxygenase-1 induction by NRF2 requires inactivation of the transcriptional repressor BACH1. *Nucleic Acids Res*. 2007;35:7074–7086.

63. Martin D, Rojo AI, Salinas M, et al. Regulation of heme oxygenase-1 expression through the phosphatidylinositol 3-kinase/Akt pathway and the Nrf2 transcription factor in response to the antioxidant phytochemical carnosol. *J Biol Chem*. 2004;279:8919–8929.

64. Konrad FM, Braun S, Ngamsri KC, Vollmer I, Reutershan J. Heme oxygenase-1 attenuates acute pulmonary inflammation by decreasing the release of segmented neutrophils from the bone marrow. *Am J Physiol Lung Cell Mol Physiol*. 2014;307:L707–L717.

65. Cai C, Teng L, Vu D, et al. The heme oxygenase 1 inducer (CoPP) protects human cardiac stem cells against apoptosis through activation of the extracellular signal-regulated kinase (ERK)/NRF2 signaling pathway and cytokine release. *J Biol Chem*. 2012;287:33720–33732.

66. Schumacher A, Wafula PO, Teles A, et al. Blockage of heme oxygenase-1 abrogates the protective effect of regulatory T cells on murine pregnancy and promotes the maturation of dendritic cells. *PLoS One*. 2012;7:e42301.

67. Fernandez-Mendivil C, Luengo E, Trigo-Alonso P, Garcia-Magro N, Negredo P, Lopez MG. Protective role of microglial HO-1 blockade in aging: Implication of iron metabolism. *Redox Biol*. 2021;38:101789.

68. Garcia-Ramirez M, Villarroel M, Corraliza L, Hernandez C, Simo R. Measuring permeability in human retinal epithelial cells (ARPE-19): implications for the study of diabetic retinopathy. *Methods Mol Biol*. 2011;763:179–194.

69. Utepbergenov DI, Fanning AS, Anderson JM. Dimerization of the scaffolding protein ZO-1 through the second PDZ domain. *J Biol Chem*. 2006;281:24671–24677.

70. Biswal MR, Justis BD, Han P, et al. Daily zeaxanthin supplementation prevents atrophy of the retinal pigment epithelium (RPE) in a mouse model of mitochondrial oxidative stress. *PLoS One*. 2018;13:e0203816.

71. Hashizume K, Hirasawa M, Imamura Y, et al. Retinal dysfunction and progressive retinal cell death in SOD1-deficient mice. *Am J Pathol*. 2008;172:1325–1331.

72. Sheth P, Basuroy S, Li C, Naren AP, Rao RK. Role of phosphatidylinositol 3-kinase in oxidative stress-induced disruption of tight junctions. *J Biol Chem*. 2003;278:49239–49245.

73. Rao RK, Basuroy S, Rao VU, Karnaky KJ, Jr, Gupta A. Tyrosine phosphorylation and dissociation of occludin–ZO-1 and E-cadherin–β-catenin complexes from the cytoskeleton by oxidative stress. *Biochem J*. 2002;368:471–481.

74. Chi Y, Zhang X, Zhang Z, et al. Connexin43 hemichannels contributes to the disassembly of cell junctions through modulation of intracellular oxidative status. *Redox Biol*. 2016;9:198–209.

75. Sliwinski T, Kolodziejska U, Szaflik JP, Blasiak J, Szaflik J. Association between the 25129A > C polymorphism of the nuclear respiratory factor 2 gene and age-related macular degeneration. *Klin Oczna*. 2013;115:96–102.

76. Synowiec E, Szaflik J, Chmielewska M, et al. An association between polymorphism of the heme oxygenase-1 and -2 genes and age-related macular degeneration. *Mol Biol Rep*. 2012;39:2081–2087.